Tumor immune microenvironment of primary prostate cancer with and without germline mutations in homologous recombination repair genes

Anna Sofia Trigos [1,2] Anupama Pasam,[1] Patricia Banks,[3] Roslyn Wallace,[3] Christina Guo,[4,5] Simon Keam [1,2] Heather Thorne,[1,2] kConFab,[1,2] Catherine Mitchell,[6] Stephen Lade,[6] David Clouston,[7] Alexander Hakansson,[8] Yang Liu,[8] Benjamin Blyth,[1,2] Declan Murphy,[2,9] Nathan Lawrentschuk,[2,3] Damien Bolton,[10] Daniel Moon,[3] Phil Darcy,[1,2] Ygal Haupt,[1,2] Scott G Williams,[11] Elena Castro,[12] David Olmos,[12,13] David Goode,[1,2] Paul Neeson [1,2] Shahneen Sandhu[1,2,3]

Correspondence to
Dr Shahneen Sandhu;
Shahneen.Sandhu@petermac.org

ABSTRACT

Background Aberrations in homologous recombination repair (HRR) genes are emerging as important biomarkers for personalized treatment in prostate cancer (PCa). HRR deficiency (HRD) could affect the tumor immune microenvironment (TIME), potentially contributing to differential responses to poly ADP-ribose polymerase (PARP) inhibitors and immune checkpoint inhibitors. Spatial distribution of immune cells in a range of cancers identifies novel disease subtypes and is related to prognosis. In this study we aimed to determine the differences in the TIME of PCa with and without germline (*g*) HRR mutations.

Methods We performed gene expression analysis, multiplex immunohistochemistry of T and B cells and quantitative spatial analysis of PCa samples from 36 patients with *g*HRD and 26 patients with sporadic PCa. Samples were archival tumor tissue from radical prostatectomies with the exception of one biopsy. Results were validated in several independent cohorts.

Results Although the composition of the T cell and B cells was similar in the tumor areas of *g*HRD-mutated and sporadic tumors, the spatial profiles differed between these cohorts. We describe two T-cell spatial profiles across primary PCa, a clustered immune spatial (CIS) profile characterized by dense clusters of CD4+ T cells closely interacting with PD-L1+ cells, and a free immune spatial (FIS) profile of CD8+ cells in close proximity to tumor cells. *g*HRD tumors had a more T-cell inflamed microenvironment than sporadic tumors. The CIS profile was mainly observed in sporadic tumors, whereas a FIS profile was enriched in *g*HRD tumors. A FIS profile was associated with lower Gleason scores, smaller tumors and longer time to biochemical recurrence and metastasis.

Conclusions *g*HRD-mutated tumors have a distinct immune microenvironment compared with sporadic tumors. Spatial profiling of T-cells provides additional information beyond T-cell density and is associated with time to biochemical recurrence, time to metastasis, tumor size and Gleason scores.

WHAT IS ALREADY KNOWN ON THIS TOPIC

⇒ Prostate cancer (PCa) is generally an immunologically cold tumor. Patients with PCa with homologous recombination repair deficiency (HRD) have shown improved responses to immune checkpoint inhibition (ICI) compared with non-HRD cancers, but to date, the molecular basis of this difference has not been elucidated.

WHAT THIS STUDY ADDS

⇒ We profiled the tumor immune microenvironment of PCas with germline mutations in homologous recombination repair genes for the first time, and show that these cancers have a more T-cell inflamed microenvironment than sporadic tumors. Further, our gene expression signature was associated with longer time to biochemical recurrence and metastasis.

HOW THIS STUDY MIGHT AFFECT RESEARCH, PRACTICE, OR POLICY

⇒ Immune spatial profiling of the microenvironment in PCa may provide prognostic information and define a subset of patients that may benefit from ICI. Our findings warrant further validation in prospective studies.

BACKGROUND

Homologous recombination repair deficiency (HRD), predominantly caused by *BRCA1/2* alterations, are enriched in metastatic castration-resistant prostate cancer (mCRPC) and serve as important biomarkers for personalized therapy. The PROfound phase III trial established a survival advantage for the poly ADP-ribose polymerase (PARP) inhibitor olaparib in mCRPC with HRD leading to regulatory approval and implementation of

mainstream molecular testing and personalized treatment in a subset of mCRPC patients. Notably, the response rate for PARP inhibitors in *BRCA1/2* altered tumors was consistently 40%–50% across multiple trials,[1–3] implying the presence of genomic alterations in the homologous recombination repair (HRR) pathway alone may be insufficient to predict responses. Biallelic deletions, loss of heterozygosity of the wild type allele,[4] functional implications of the specific variant, co-occurring genomic alterations and other factors such as the tumor immune microenvironment (TIME) may potentially contribute to the differential responses observed. In breast and ovarian cancer, response to programmed death 1 (PD-1/PD-ligand 1 (PD-L1)) inhibition is enriched in tumors with germline (g) *BRCA1/2* mutations and these tumors have been shown to harbor higher tumor mutational load, lymphocyte infiltration and tumor-specific neoantigens for immune activation.[5–8] In the KEYNOTE-199 and Checkmate 650 trials, HRD in prostate cancer (PCa) were also associated with higher and more durable responses to immune checkpoint inhibitors (ICI)[9 10] although the biological basis for this observation is poorly understood. Currently, we lack an understanding of the TIME of PCa in patients with *g*HRD mutations, and how this differs from that of sporadic tumors.

PCa is generally considered an immunologically cold tumor.[11] While a higher tumor immune infiltration has been associated with better immune control and prognosis in other cancers,[12] studies in PCa have revealed conflicting results, with higher T-cell levels in tumor areas associated with better prognosis in some studies,[13 14] but worse in others.[15–19] Possible explanations include heterogeneity between cohorts, the complexity of the spatial interactions between immune and tumor cells and generally low levels of immune infiltration that make the application of the classical definitions of immune infiltrated or excluded tumors challenging. In melanoma, sarcoma and breast cancer, complex spatial patterns of distinct immune subsets in the stroma and tumor-immune interactions have been linked to overall survival and response to immunotherapy.[20–26] Further studies of the interface between tumor genomics and the TIME are warranted to understand how best to personalize therapies. Herein we profiled the density and spatial distribution of T and B cells in primary PCa with and without *g*HRD in tumor and surrounding stroma using gene expression and quantitative spatial analysis.

METHODS
Sample cohort
Our cohort consisted of 62 primary PCa samples. Twenty-six samples were from patients with *gBRCA2* mutations, five from patients with *gBRCA1* mutations, a double *gBRCA2+gMSH2* carrier and four with other *g*DNA repair mutations (*ATM, FANCI, PALB2, CHEK2*, n=1 of each) (figure 1, online supplemental methods). We refer to the cohort with germline alterations in HRR genes hereafter
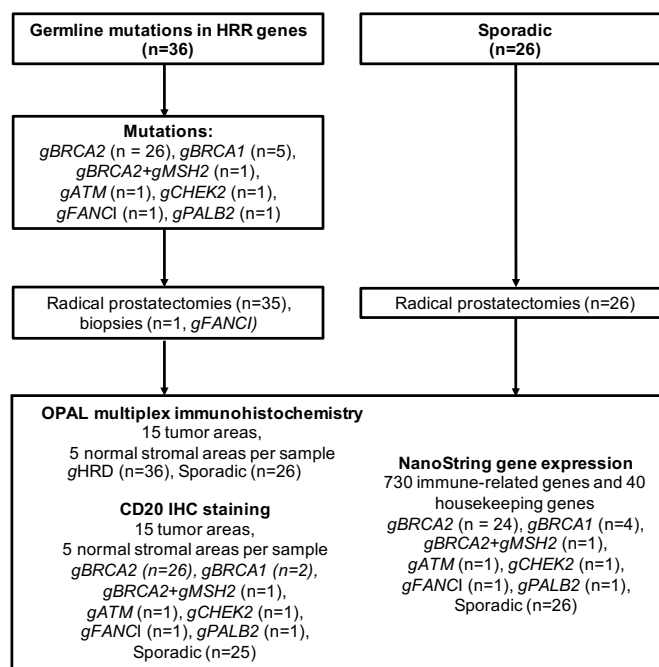

Figure 1 Study flow chart. Our study includes 36 samples from primary PCa with germline mutations in HRR genes and 26 from patients with sporadic PCa. All samples underwent OPAL mIHC. Thirty-three HRD and 26 sporadic samples passed quality control for NanoString gene expression analysis. HRD, homologous recombination repair deficiency; HRR, homologous recombination repair; *g*, germline; n, number of samples; mIHC, multiplex immunohistochemistry; PCa, prostate cancer.

as the HRD cohort/tumors. An additional 26 were primary PCa samples from patients without *g*DNA repair mutations based on germline testing using an established targeted DNA repair panel of 26 genes and are referred hereafter as 'sporadic'. All samples were radical prostatectomies, except for the *gFANCI* sample which was a prostate biopsy, thereby enabling a comprehensive evaluation of the TIME in whole prostates. Clinical characteristics of the cohort and germline variants are outlined in online supplemental tables S1 and S2.

Gene expression
We used the NanoString nCounter PanCancer Immune Profiling Panel comprizing of 730 immune-related genes and 40 housekeeping genes. RNA was extracted from formalin fixed paraffin embedded (FFPE) sections using the RNAeasy FFPE kit (Qiagen). Fifty-nine samples were evaluable. One *gBRCA1* and two *gBRCA2* samples were excluded from the gene expression analyses due to poor RNA quality. We performed differential expression analyses and investigated the expression of specific signatures such as the tumor inflammation signature (TIS)[27] which measures a T-cell inflamed tumor microenvironment that has previously been shown to correlate with response to PD-1/L1 blockade. We also evaluated the tissue-resident memory (TRM) T-cell signature which is implicated in maintaining immunity.[28]

Multiplex immunohistochemistry

Given the prevalence of TIS and TRM signatures in the HRD cohort, seven-color OPAL multiplex immunohistochemistry (mIHC) was used to quantify $CD3^+CD4^+$ (helper T cells), $CD3^+CD8^+$ (cytotoxic T cells), $CD3^+CD4^+FOXP3^+$ (regulatory T cells (Tregs)), tumor cells ($AMACR^+$) and $PD-L1^+$ cells (online supplemental methods). Tumor areas were marked by a pathologist. Fifteen representative multispectral images of the tumor area and five of normal stromal tissue outside of the tumor area (adjacent to the tumor and distant from the tumor) were obtained to gain a comprehensive representation of the tumor and stroma within whole prostatectomy (n=62) and tumor biopsy (n=1) samples. These selected regions are referred to as regions of interest (ROI).

CD20 immunohistochemistry

To better understand the spatial distribution of B cells and the formation of tertiary lymphoid structures (TLS), we performed 3,3'-diaminobenzidine (DAB)-staining of B-cells with CD20 (Clone L26, Agilent Technologies) and dendritic cells with CD21 (Clone 1G9, Novocastra antibody, Leica) in serial sections of the same sample set used for OPAL mIHC. Slides were scanned on the VS120 slide scanner (Olympus) and analyzed for the presence of DAB-positive cells using the CellSens Dimension Desktop software (Olympus). After co-registering the DAB-stained and OPAL-stained images, we matched the 15 fields in the tumor area and 5 in the normal stromal tissue to those selected in the OPAL T cell panel. The presence and number of B cells per ROI was then indexed to the mIHC data. Identification of TLS was carried out with the aid of an expert hematopathologist based on morphology and size (an area of at least $2000\,\mu m^2$) of the B cell aggregates and the CD21 staining to define the follicular architecture.

Spatial analysis

Spatial analysis of the immune microenvironment was carried out using the SPIAT R package, which was developed inhouse for the spatial image analysis of cells in tissues.[29] Only images with at least 100 tumor cells were considered for the tumor area analyses. Clusters of $CD3^+CD4^+$, $CD3^+CD8^+$, $CD3^+CD4^+FOXP3^+$, $CD3^+CD4^-CD8^-$ and $AMACR^-PD-L1^+$ cells were defined using a previously described custom algorithm.[29] To identify clusters, first we calculated the distance between all T and $AMACR^-PD-L1^+$ cells in all images. The top 0.5% pairs of closest cells were regarded as being neighbors. Groups of neighboring cells within the same image were defined as aggregates. Visual inspection confirmed such aggregates were clearly evident. Each of these individual aggregates were considered 'clusters' in our analysis if comprised of at least 50 cells. Cells not in clusters or in aggregates of less than 50 cells were considered 'free'. A cut-off of 50 was selected based on the distribution of the composition of cell types, where cells in aggregates of less than 50 cells had a similar composition to those that were not

in aggregates, whereas those of more than 50 cells had a composition more consistent with those in larger clusters. Visual inspection also supported that intuitively 50 cells corresponded to a clearly identifiable cluster of cells. Mann-Whitney tests were used to test for statistical significance. One-sided tests were used to test for differences in a specified direction.

Validation cohorts

The association between gene expression signatures, tumor size, Gleason score and Kaplan-Meier analysis for time to biochemical recurrence and metastasis were validated in four large independent cohorts of primary PCas with gene expression data: 497 samples from The Cancer Genome Atlas (TCGA),[30] 73 from the Fraser *et al* cohort,[31] 8635 from the Decipher GRID database,[32] including 855 from a meta-analysis of radical prostatectomy (RP) patients from the Spratt *et al* cohort,[33] 545 of RP patients from the Erho *et al* cohort[34] (both with available survival outcomes data) and 7235 from RP patients obtained from clinical use of the Decipher test ordered by physicians between 2013 and 2017 (with baseline pathology information) as previously described.[32]

RESULTS

HRD tumors have a more inflamed TIME than sporadic tumors

We performed differential expression analysis between HRD and sporadic tumors to understand differences in the TIME profile. We obtained 190 differentially expressed genes (adjusted p value <0.05) (figure 2A). Upregulated genes in the HRD cohort included B-cell markers (CD79A, CD79B, MS4A1), the immune checkpoint CD96, as well as cytokines and chemokines (CXCL13, CXCL9, CXCL10) (online supplemental table S3). The most highly differentially expressed gene in the HRD cohort was the Major Histocompatibilty Complex (MHC) Class I molecule Human Leukocyte Antigen (HLA)-A, which is required for immune recognition by cytotoxic effector T cells (fold change=2.60, p value adjusted for multiple testing using Benjamini-Hochberg Procedure=3.66×10^{-8}) (figure 2A,B). To investigate whether there was a T-cell–inflamed TIME in the HRD cohort, we used the TIS, which has previously been shown to measure tumor inflammation and enhanced responses to ICI.[27] HRD samples had higher TIS levels than sporadic tumors (one-sided Mann-Whitney test p value=8.12×10^{-5}) (figure 2C, online supplemental figure S1A). HRD samples also had higher levels of a TRM T-cell signature[28] (one-sided Mann-Whitney test p value=0.00051) (figure 2D, online supplemental figure S1B), which is linked to immunosurveillance, improved prognosis and ICI modulation.[28 35] Overall, the HRD tumors had a more T-cell–inflamed TIME than sporadic tumors.

T-cell densities in the TIME of HRD and sporadic tumors

To investigate the composition of T cells within tumors, we used seven-color OPAL mIHC to characterize helper
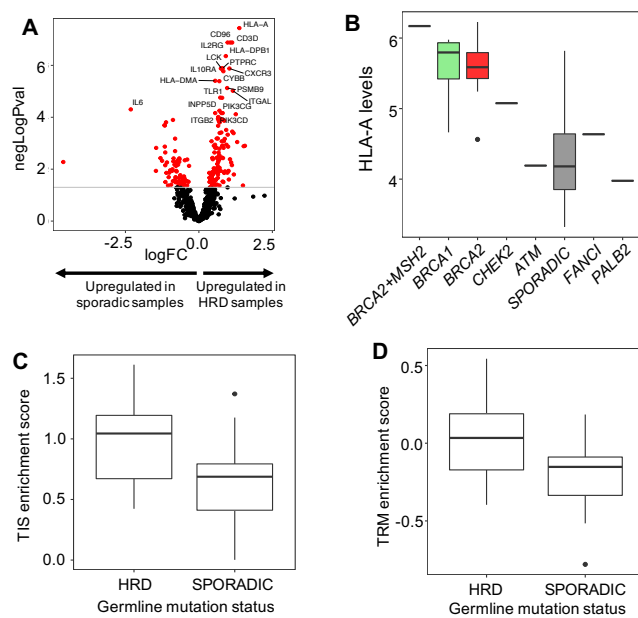
Figure 2 Gene expression analysis of HRD and sporadic tumors. (A) Differential gene expression between HRD and sporadic tumor samples. There were 190 differentially expressed genes, including 125 upregulated in HRD tumors, and 65 upregulated in sporadic tumors. Red dots correspond to genes with adjusted p values<0.05. The horizontal line corresponds to an adjusted p value of 0.05. (B) Gene expression levels of HLA-A in HRD and sporadic tumors. HLA-A were higher in HRD tumors, although *gATM*, *gFANCI* and *gPALB2* samples had lower levels than *gBRCA2* and *gBRCA1* tumors (fold change=2.60, adjusted p value=3.66×10^{-8}). (C) Tumor inflammation signature (TIS) in HRD and sporadic tumors. HRD tumors had significantly higher TIS levels (one-sided Mann-Whitney test p value=8.12×10^{-5}), indicating a more inflamed T-cell microenvironment. (D) Tissue-resident memory T-cell (TRM) signature in HRD and sporadic tumors. HRD tumors had significantly higher TRM signature levels (one-sided Mann-Whitney test p value=0.00051), indicating a more inflamed T-cell microenvironment. g, germline; HRD, homologous recombination repair deficiency; HLA-A, Human Leukocyte Antigen A.

(CD3⁺CD4⁺), cytotoxic (CD3⁺CD8⁺), regulatory (CD3⁺C-D4⁺FOXP3⁺) and double negative (CD3⁺CD4⁻CD8⁻) T-cell populations (figure 3A). T-cell density of the tumor area was heterogeneous across cohorts (figure 3B,C and online supplemental figure S2) (43.93 to 1089.01 cells/mm² in HRD samples and 48.06 cells/mm² to 2,161.14 cells/mm² in sporadic samples) (figure 3D). The tumor area of HRD samples had lower T-cell densities (median of 303.91 cells/mm²) compared with those of sporadic samples (433.99 cells/mm²), although this difference was not statistically significant (Mann-Whitney test p value=0.14). There was enrichment of T cells in the tumor area compared with non-tumor areas in 18/26 *gBRCA2* samples, 20/26 sporadic, 4/5 *gBRCA1* and in the *gATM, gCHEK2, gFANCI, gPALB2, gBRCA2+gMSH2* samples (figure 3E).

T-cell density heterogeneity was associated with the type of the mutated gene in HRD tumors. *gBRCA2* tumors had a median of 368.90 cells/mm² (range=52.57–1089.00 cells/mm²). *gBRCA1* tumors clustered towards the lower range of the spectrum in the HRD cohort (median=184.28 cells/mm², range=43.93–288.01 cells/mm²), as did tumors with germline mutations in *gFANCI, gATM, gPALB2* and *gCHEK2* (54.47, 79.80, 151.10 and 347.17 cells/mm², respectively). Levels of T cells in the *gBRCA2+gMSH2* tumor was similar to *gBRCA1* and *gBRCA2* samples (173.35 cells/mm²) (figure 3D).

The composition of the T cell population in the tumor areas was similar across both cohorts (figure 3F,G and online supplemental figure S3). CD4⁺ T cells were the most common subtype, representing a median of 69.78% and 70.08% of the T-cell population in the HRD and sporadic cohorts, respectively. This was followed by CD8⁺ T cells (25.47% for HRD, 26.49% for sporadic), double negative T cells (3.22% for HRD, 1.65% for sporadic), and Tregs (0% for HRD, 0.46% for sporadic). *gBRCA2* had similar percentages of CD8⁺ T cells to sporadic tumors (Mann-Whitney test p value=0.82), and similar CD8⁺/CD4⁺ ratios (Mann-Whitney test p value=0.96). However, *gBRCA1* tumors had a higher percentage of CD8⁺ T cells than *gBRCA2* tumors (one-sided Mann-Whitney test p value=0.018), and a higher CD8⁺/CD4⁺ ratio (one-sided Mann-Whitney test p value=0.013). The double carrier *gBRCA2+gMSH2* tumor had the highest proportion of CD8⁺ T cells (50.77%), consistent with previous reports for tumors with mismatch repair mutations.[36]

PD-L1⁺ cells were rare across cohorts

Since tumor PD-L1 expression is currently approved as a predictive biomarker for PD-L1 blockade in several cancers, and HRD tumors had higher TIS scores, a potential predictor of response to PD-1/PD-L1 blockade,[27] we investigated the presence PD-L1⁺ cells. PD-L1⁺ tumor and non-tumor cells were rare across both cohorts, consistent with previous reports.[37] Only 1/26 *gBRCA2* and 4/26 sporadic samples had more than 1% PD-L1⁺ stromal cells (online supplemental figure S4A,B). Similarly, only 2/26 sporadic and 2/26 *gBRCA2* samples had more than 1% PD-L1⁺ tumor cells (online supplemental figure S4C,D).

Spatial distribution of tumor-infiltrated T cells

Despite similar T-cell density and composition between the two cohorts, T cells displayed distinct spatial profiles across tumors. In some tumor areas, T cells were aggregated into clusters (figure 4A), while in others T cells were individually scattered across the tumor area (figure 4B). We refer to these patterns as the cluster immune spatial (CIS) profile characterized by 'clustered' T cells largely in the stromal area, and the free immune spatial (FIS) profile, characterized by 'free' T cells largely in the tumor regions. To quantify these patterns, we performed spatial analysis using SPIAT,[29] which allowed identifying immune cells forming clusters from those that were freely
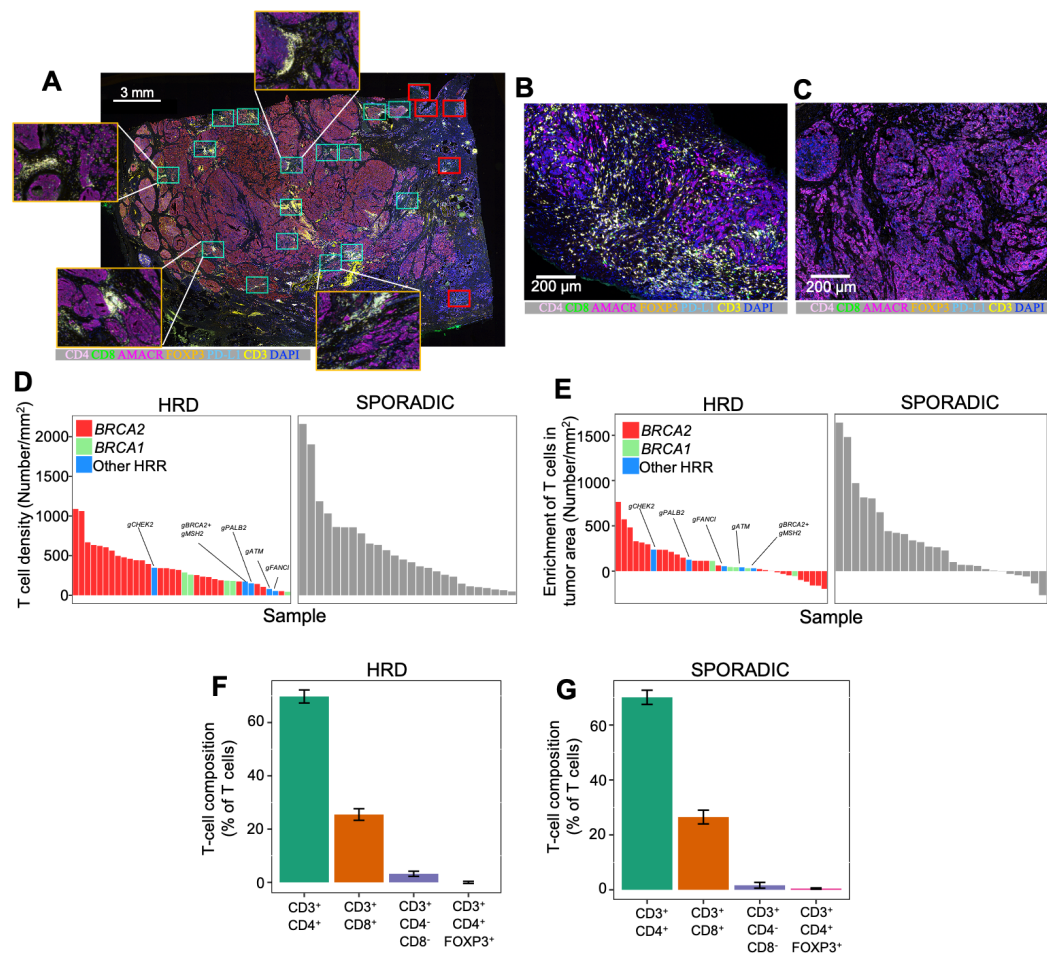
Figure 3 The T-cell and PD-L1 composition of the microenvironment of primary prostate tumors with and without HRD. (A) OPAL mIHC of tissue sections. Tumor and stromal regions were marked by a pathologist. Fifteen representative tumor areas (blue squares) and five representative normal stromal areas (red squares) of 1.3 mm^2 were selected from each tissue section. (B and C) OPAL mIHC of *gBRCA2* tumors with high (B) and low levels (C) of T cell, indicating a range of T cell densities in the microenvironment. (D) Density of T cells across the cohorts. HRD tumors tended to have lower T-cell densities, although the difference was not statistically significant. (E) Enrichment of T cells in the tumor area. Values greater than 0 indicate a higher density of T cells in the tumor area, whereas values lower than 0 indicate depletion. The majority of samples in both cohorts (77% of sporadic samples and 75% of HRD samples), are enriched in T cells in the tumor area. (F and G) Composition of T-cell populations in HRD (F) and sporadic cohorts (G). CD3$^+$CD4$^+$ cells were the most common, followed by CD3$^+$CD8$^+$ cells and CD3$^+$CD4$^-$CD8$^-$ cells. CD3$^+$CD4$^+$FOXP3$^+$ were rare in our cohort. Values depicted are medians±SE. g, germline; HRD, homologous recombination repair deficiency; mIHC, multiplex immunohistochemistry.

distributed across the tissue (see Methods) and characterizing their composition.

The predominant pattern of CIS and FIS profiles differed between HRD and sporadic cohort, implying that T-cell density alone may be insufficient to understand the biological implications of T cells in PCa. To quantify the CIS profile in each patient, we averaged the number of clusters across each of the ROIs selected in the tumor area for each patient. HRD tumors had fewer clusters, with a median of 0.48 clusters/mm^2 compared with 1.06 clusters/mm^2 in sporadic tumors (one-sided Mann-Whitney test p value=0.024) (figure 4C). In contrast, HRD tumors had significantly more free T cells infiltrating the tumor compared with sporadic tumors. The median ratio of the free/clustered cells per mm^2 was 67.71 in HRD tumors compared with 48.34 in sporadic

tumors (one-sided Mann-Whitney test p value=0.0039). This ratio may infer the degree to which T cells are available to interact with tumor cells (figure 4D). In 13/36 (36.11%) of HRD tumors (10/26 *gBRCA2*, 2/5 *gBRCA1* and the *gBRCA2+gMSH2* tumor) the free/clustered ratio was higher than in any of the sporadic tumors (figure 4D). Notably, HRD tumors also had higher percentages of free CD8$^+$ T cells compared with sporadic tumors (one-sided Mann-Whitney test p value=0.015) (figure 4E), whereas sporadic tumors had higher levels of clustered CD8$^+$ T cells (one-sided Mann-Whitney test p value=0.015) (figure 4F).

Formation of TLS

Given the higher expression of B cell markers in the HRD cohort, we next investigated how the T cell spatial profiles
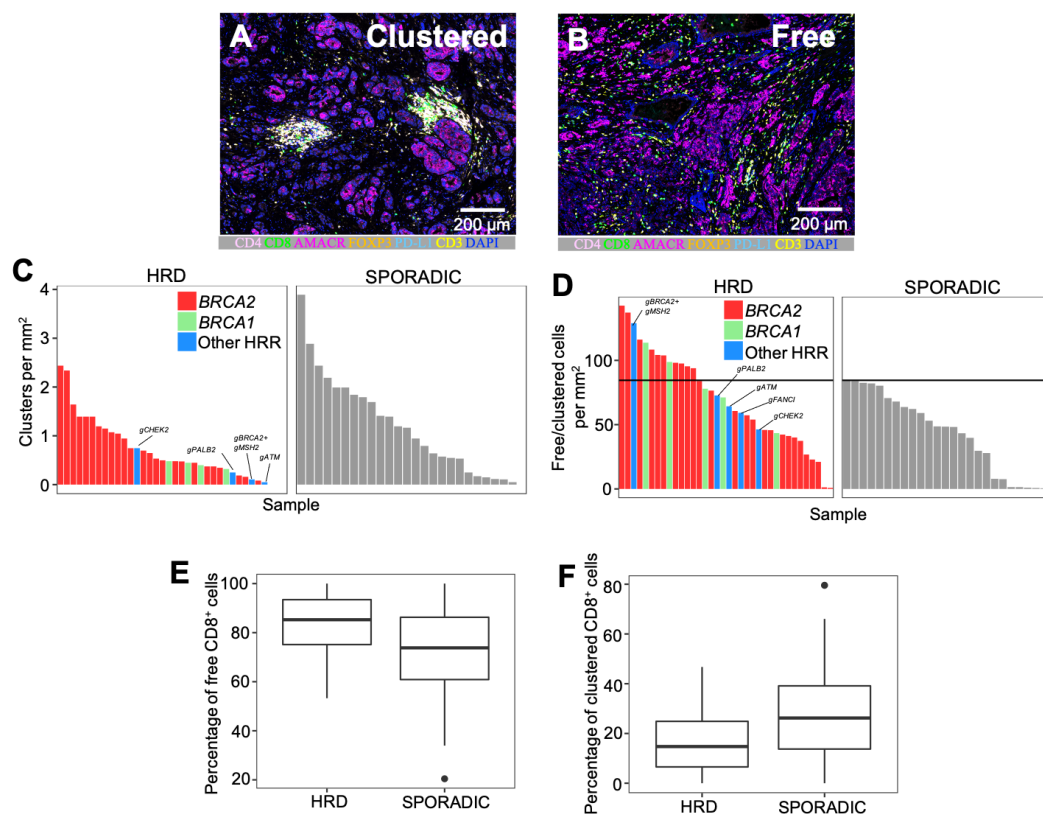
Figure 4 Clustered and free immune spatial profiles. (A) mIHC image depicting an example of a CIS profile within the tumor region in a sporadic tumor. T cells are aggregated in a cluster away from tumor cells. (B) An example of a FIS profile within the tumor region of a *gBRCA2* tumor. T cells are freely distributed and interacting with tumor cells. (C) Density of clusters of T cells in HRD and sporadic tumors. HRD tumors are depleted of clusters compared with sporadics. (D) Ratio of free to clustered cells per mm^2. HRD tumors have overall higher levels of the free/clustered cell ratio. The horizontal line indicates the maximum ratio in sporadic. (E) Percentage of free CD8$^+$ T cells in HRD and sporadic tumors. The percentage of free CD8$^+$ T cells is higher in HRD tumors compared with sporadic tumors (one-sided Mann-Whitney test p value=0.015). (F) Percentage of clustered CD8$^+$ T cells in HRD and sporadic tumors. The percentage of clustered CD8$^+$ T cells is higher in sporadic tumors compared with HRD tumors (one-sided Mann-Whitney test p value=0.015). FIS, free immune spatial; CIS, clustered immune spatial; g, germline; HRD, homologous recombination repair deficiency; mIHC, multiplex immunohistochemistry.

(CIS and FIS) associated with B cells and if these B cells formed TLS within the tumor and/or stromal regions. We performed immunohistochemistry (IHC) staining for CD20 to investigate the density of B-cells across HRD and sporadic samples. Overall, B cells were significantly rarer than T cells in the tumor areas of both cohorts (medians of 341.99 T cells/mm^2, 32.61 B cells/mm^2, one-sided Man-Whitney test p=1.16×10^{-9} in HRD tumors, and 416.74 T cells/mm^2, 36.99 B cells/mm^2, p=5.96×10^{-8} in sporadic tumors) (figure 5A,B). There were no statistical differences in the B-cell density in tumor areas of *gBRCA2* and sporadic samples (median density in *gBRCA2* samples=46.31 cells/mm^2, sporadic tumors=36.99 cells/mm^2, Mann-Whitney test p value=0.81) (figure 5C).

There was a higher density of B cells in the tumor area of sporadic samples compared with the stroma (one-sided Mann-Whitney paired test p value=0.00065). In contrast, the B cell density in the surrounding stroma of *gBRCA2* samples was similar to that found in its tumor areas (median in stroma=36.79 cells/mm^2, median in

tumor area=46.31 cells/mm^2, Man-Whitney paired test p value=0.56). In fact, the density of B cells in the stroma of *gBRCA2* samples was higher than that in sporadic samples (median density in *gBRCA2* samples=36.79 cells/mm^2, median density in sporadic samples=11.75 cells/mm^2, one-sided Man-Whitney test p value=0.032) (figure 5D). This higher density of B-cells in the stroma of *gBRCA2* samples might account for the overexpression of B cell markers in the HRD cohort (figure 2A).

A similar proportion of sporadic and *gBRCA2* samples displayed no B cells in their tumor area (3/25 sporadic and 4/26 *gBRCA2* samples), but had no unique clinical characteristics. One of the two profiled *gBRCA1* samples did not display B cells, and the other only had a density of 23.56 cells/mm^2 in the tumor area and 14.92 cells/mm^2 in the stromal area. The *gCHEK2*, *gFANCI* and *gPALB2* tumors had no B cells, and the *gATM* and *gBRCA2+gMSH2* samples had similarly low levels (24.57 cells/mm^2 in the tumor area and 7.46 cells/mm^2 in the stromal area of the *gATM* sample, and 21.93 cells/mm^2 in
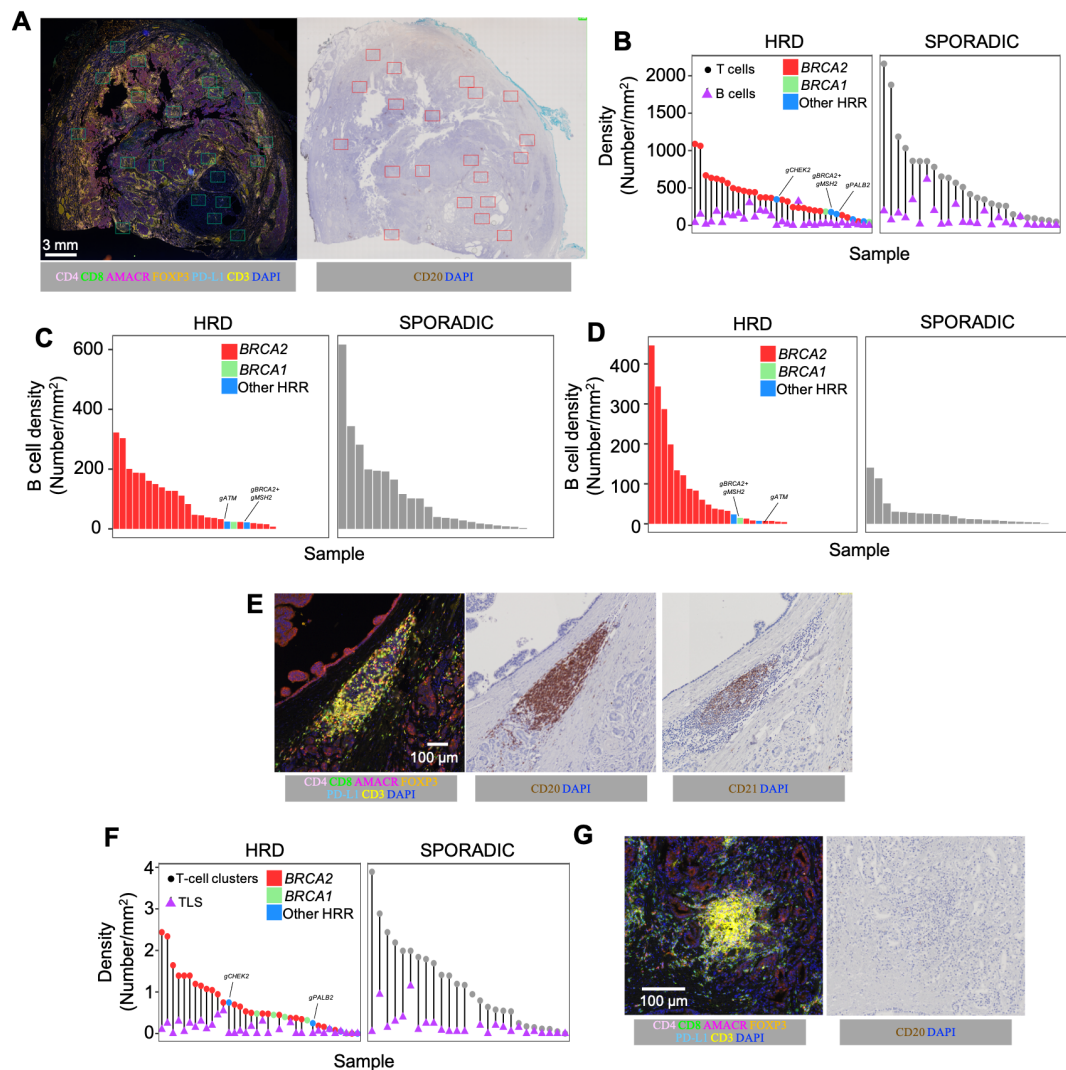
Figure 5 B cells and TLS in the HRD and sporadic cohorts. (A) Example multiplex IHC of the OPAL T cell panel (left) and IHC of CD20, B cells (right). T cells are more common than B cells. (B) Density of T cells and B cells in HRD and sporadic tumors. B cells are rarer than T cells in both cohorts (Mann-Whitney p value=1.16×10^{-9} in HRD tumors and 5.96×10^{-8} in sporadic tumors). (C) Density of B cells in the tumor area of HRD and sporadic samples. *gBRCA2* tumors have similar B cell densities to sporadic tumors (two-sided Man-Whitney test p value=0.81). (D) Density of B cells in the stromal area of HRD and sporadic samples. *gBRCA2* tumors had higher levels of B cells in the stromal area compared with sporadic tumors (one-sided Man-Whitney test p value=0.032). (E) Example TLS in a sporadic sample, showing the classical pattern of T cells (left) surrounding dense B-cell regions (middle), with a core of dendritic cells (right) forming the follicular structure. (F) Density of T cell clusters and TLS across the cohorts. The density of T cell clusters is consistently larger than that of TLS. (G) Clusters of T cells with no accompanying B cell staining. *g,* germline; HRD, homologous recombination repair deficiency; IHC, immunohistochemistry; TLS, tertiary lymphoid structures.

the tumor area and 23.58 cells/mm^2 in the stromal area of the *gBRCA2+gMSH2* sample). Overall, the tumor areas of HRD tumors were not enriched in B cells, although these tumors had higher levels of B cells in the surrounding stroma compared with sporadic tumors.

We identified TLS based on CD20 staining and used CD21 to verify follicular architecture (figure 5E). Despite HRD samples displaying a FIS profile, we observed the presence of TLS in the tumor area of 65.38% (17/26) of *gBRCA2* samples and in the *gATM* and *gBRCA2+gMSH2* tumors. This was similar to the percentage found in sporadic samples (76.00%, 19/25). However, the median

density across the cohorts was low (0.057 TLS/mm^2 in the tumor area and 0 TLS/mm^2 in the stroma area of HRD samples, 0.079 TLS/mm^2 in the tumor area and 0 TLS/mm^2 in the stroma area of sporadic samples). There were no differences in the TLS density of sporadic and HRD samples in the tumor area (Mann-Whitney test p value=0.40) or stromal areas (Mann-Whitney test p value=0.61).

Clusters of T cells associated with a CIS profile were significantly more common than TLS (figure 5F) (one-sided paired Mann-Whitney p value=1.35×10^{-6} for HRD tumors and 9.70×10^{-6} for sporadic tumors), with the

majority of T cell clusters not co-localizasing with B cells (figure 5G). T cell clusters were more common than TLS in sporadic and HRD tumors with TLS (median of 7.20 and 4.67 times, respectively). This points towards the likely formation of a CIS profile as a distinct process to the formation of TLS.

Finally, we investigated whether B cell or TLS density were associated with clinical outcome. We found no significant association with time to biochemical recurrence, time to metastasis, or survival with either density of B cells or density of TLSs (p values=0.99, 0.5, 0.97, and 0.88, 0.78, 0.87, respectively).

The free and clustered T-cell populations

The distribution of T-cell subtypes was distinct between the clustered and free populations. As T cell clusters got bigger (included more cells), there was a higher proportion of CD4$^+$ T cells (one-sided Jonckheere Telspra (JT) test p=3.74×10^{-4}) (figure 6A), whereas the percentage of CD8$^+$ T cells decreased (one-sided JT test p=2.25×10^{-8}) (figure 6B). In contrast, a higher percentage of free T cells within the tumor were CD8$^+$ compared to the clustered T cell population (one-sided paired Mann-Whitney test p value=7.75×10^{-10}) (figure 6C), and a lower percentage
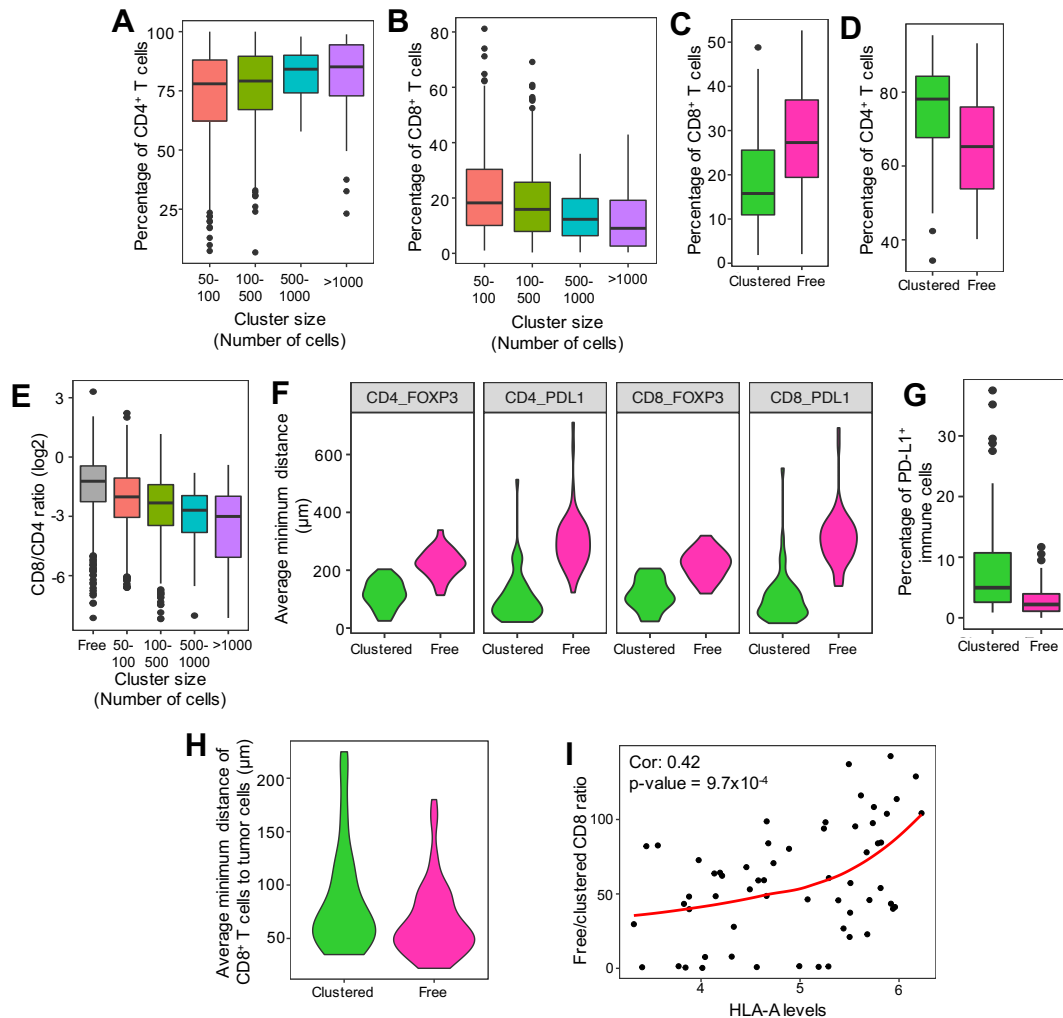

Figure 6 Clustered and free immune spatial profiles. (A) Percentage of CD4$^+$ T cells in immune clusters. Larger clusters have higher percentages of CD4$^+$ cells, suggesting functional aggregation of CD4$^+$ T cells. (B) Percentage of CD8$^+$ T cells in immune clusters. Larger cluster have lower percentages of CD8$^+$ cells, indicating a depletion of these cells. (C and D) Comparison of CD4$^+$ and CD8$^+$ T cells in the clustered and free populations. There are higher levels of CD8$^+$ cells in the free T cell populations, but higher levels of CD4$^+$ cells in the clustered population. (E) Ratio of CD8$^+$/CD4$^+$ cells (log2) in free and clustered cells of different size. Larger clusters tended to have a lower CD8$^+$/CD4$^+$ ratio. (F) Average minimum distances between CD4$^+$ and CD8$^+$ T cells with Tregs and PD-L1$^+$ stromal cells. CD4$^+$ and CD8$^+$ T cells are more closely interacting with Tregs and PD-L1$^+$ stromal cells in clusters than when they are freely distributed, pointing towards an inhibitory environment in the immune clusters. (G) Percentage of PD-L1$^+$ stromal cells in clusters and in freely distributed cells. Clusters are enriched in PD-L1$^+$ cells compared with free cells. (H) The average minimum distance from CD8$^+$ T cells to tumor cells is shorter in the free T cell population compared with the clustered population, indicating greater levels of tumor recognition. (I) Association between levels of HLA-A and the ratio of free/clustered CD8$^+$ T cells, showing a positive correlation (Spearman correlation=0.42, p value=9.7×10^{-4}). PD-L1, programmed death ligand 1; Treg, regulatory T cells; HLA-A, Human Leukocyte Antigen A.

were $CD4^+$ (p value=5×10^{-8}) (figure 6D). The $CD8^+/CD4^+$ cell ratios were higher in free cells compared with clustered cells (JT one-sided test p<2.2×10^{-16}) (figure 6E). Given the established roles of $CD4^+$ T and $CD8^+$ T cells, free and clustered T cell populations likely have distinct biological implications.

We hypothesized that a CIS profile could be linked to a limited immune-tumor cell interaction, whereas FIS profile could be linked to higher levels of tumor immune recognition. To investigate this, we measured the distance of $CD4^+$ and $CD8^+$ T cells to Tregs and PD-L1$^+$ cells, which suppress T cell responses. The distances were shorter in the clustered compared with free T-cell populations (one-sided Mann-Whitney test p values=5.36×10^{-10} for $CD4^+$ to $CD4^+FOXP3^+$, 3.02×10^{-16} for $CD4^+$ to PD-L1$^+$, 7.23×10^{-9} for $CD8^+$ to $CD4^+FOXP3^+$, 3.05×10^{-16} for $CD8^+$ to PD-L1$^+$ cells) (figure 6F). Furthermore, PD-L1$^+$ cells were more commonly found in the clustered T-cell population (4.97% of clustered cells) than the free population (2.20%) (one-sided paired Mann-Whitney test p value=1.51×10^{-7}) (figure 6G). These results may suggest that the clustering of T cells which occurs predominantly in the stomal regions may be indicative of an immunosuppressive microenvironment.

To investigate whether the free T cell population represented a population of T cells likely involved in tumor immune recognition, we calculated the distance of free and clustered $CD8^+$ cells to tumor cells. Free $CD8^+$ cells were indeed closer to tumor cells than clustered $CD8^+$ cells (one-sided Mann-Whitney p value=0.0074) (figure 6H). Furthermore, expression of the MHC Class I molecule HLA-A required for immune recognition by cytotoxic effector T cells was positively correlated with the ratio of free to clustered $CD8^+$ T cells (Spearman correlation=0.42, p value=9.7×10^{-4}) (figure 6I), consistent with higher immune recognition.

FIS profile gene signatures predict disease aggressiveness and survival outcomes

We next hypothesized that a FIS profile might be linked to clinical characteristics of tumors. We derived a gene expression signature for the FIS profile by calculating the Spearman correlation between the ratio of free and clustered $CD8^+$ cells and the genes available in the NanoString platform and selecting the top five most highly correlated genes (*IRF7, CEACAM1, ITGAM, LILRA1* and *BAX*). There was a positive correlation between the levels of this signature and the ratio of free to clustered $CD8^+$ T cells in our cohort (online supplemental figure S5) (Spearman correlation=0.45, p value=4.07×10^{-4}), suggesting it captures a FIS profile.

Consistent with our mIHC analyses, HRD tumors had higher FIS profile signatures than sporadic samples (one-sided Mann-Whitney test p value=3.04×10^{-4}) (figure 7A). While the FIS of HRD tumors remained consistent across grade groups, there was a decreasing trend in sporadic tumors, although not significant in our cohort (decreasing JT test=0.42) (online supplemental figure S6). Using data

from 497 tumors from TCGA,[30] we found that FIS profile signature levels were higher in smaller tumors (decreasing JT p value=0.0037) and tumors with a lower Gleason score (p value=0.0046) (figure 7B,C). These trends were also found in the Fraser cohort[31] of 73 samples (online supplemental figure S7) and in the Erho *et al* cohort[34] of 545 samples (p value=10^{-5}) (figure 7D). In this cohort the FIS profile signature was higher in tumors of patients that remained free of regional or distant metastasis after RP (one-sided Mann-Whitney p value=2.06×10^{-4}) (figure 7E) and patients with a FIS profile signature above the median had longer time to metastasis (p value=0.02) (figure 7F). A similar trend was observed in the Spratt *et al* cohort of 855 patients[33] (p value=0.010) (figure 7G). Time to biochemical recurrence was longer in patients with tumors with a higher FIS profile signature in the Fraser cohort[31] (log-rank test p value=0.041) (figure 7H). Finally, in a cohort of 8635 RP patients we found higher FIS profile scores associated with lower Glinsky signature scores,[38] corresponding to the better prognosis group (JT test p<2×10^{-4}) (online supplemental figure S8). These results support our hypothesis of better accessibility of $CD8^+$ cells to tumor cells in PCas with a FIS profile that may translate into better disease control.

DISCUSSION

To our knowledge this the first study to deeply profile the spatial distribution of the TIME in up to 15 distinct areas in whole primary PCas with and without germline HRD mutations. Our results reveal several novel findings including immune gene expression signatures linked to HRD status and a complex spatial structure of the T-cell microenvironment linked to prognostic factors.

We identified a more inflamed T-cell immune microenvironment in PCas with germline HRD mutations, including cytokines, chemokines, and higher levels of the TIS and TRM gene expression signatures. Despite no significant differences in the density or composition of the tumor T-cell microenvironment between cohorts, spatial analysis revealed higher levels of free $CD8^+$ T cells that were closer to tumor cells and higher levels of HLA-A expression in the HRD cohort, potentially suggestive of better immune tumor recognition in this subset of tumors. Data from several clinical trials (Checkmate 650[39] and KEYNOTE 199[9]) have shown improved responses to immune check point inhibition in the HRD cohort.

To date most immune microenvironment studies in PCa have focused on density estimations, with studies reporting conflicting results regarding the significance of tumor immune infiltration levels,[13–19] including in tumors with *BRCA2* mutations.[40] Our quantitative spatial analyses reveal a free $CD8^+$ T cell spatial profile in the tumor area associated with positive factors for prognosis, including smaller tumor size, lower Gleason score, longer time to biochemical recurrence and onset of metastasis. This profile was more prominent in *g*HRD tumors, despite *g*HRD mutations generally being associated with
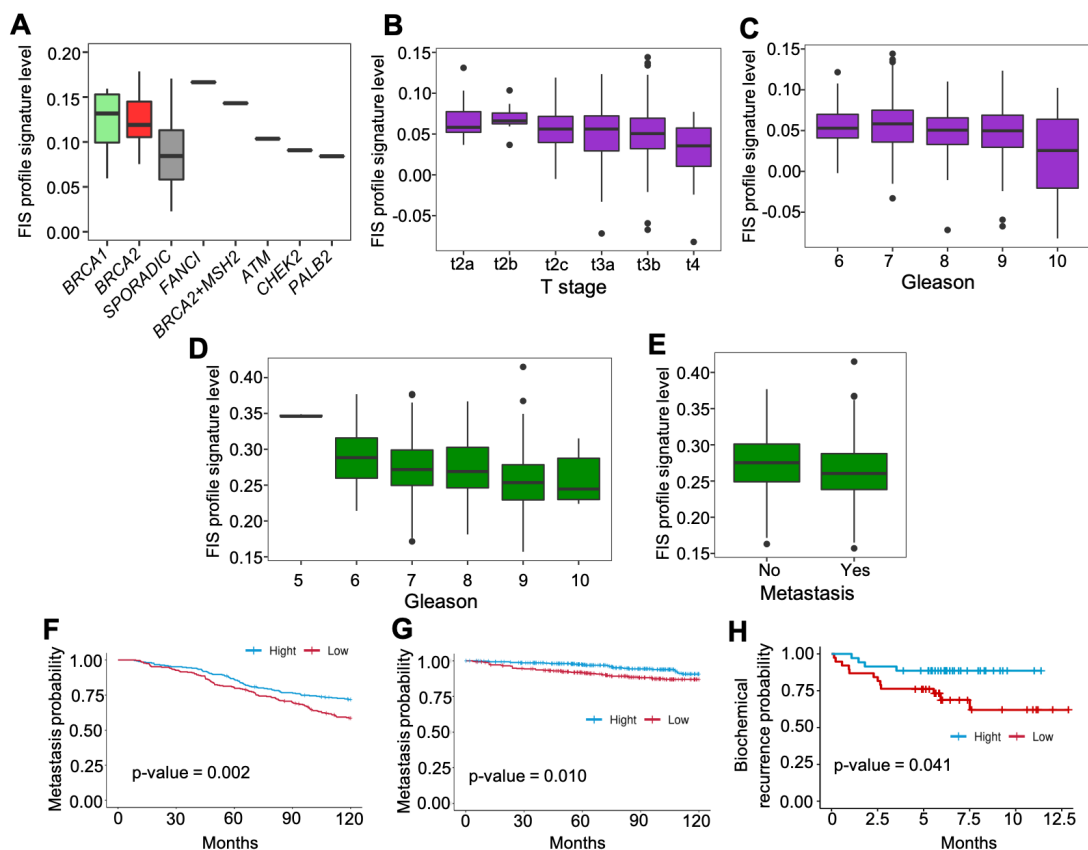
Figure 7 FIS profile gene expression signature is a marker for low grade tumors, longer time to biochemical recurrence and metastasis. (A) FIS profile signature scores across our cohort of HRD and sporadic tumors. Consistent with the multiplex immunohistochemistry results, HRD tumors have higher FIS profile scores. gBRCA1, gBRCA2 and the gFANCI and gBRCA2+gMSH2 tumors have the highest scores. gATM, gCHEK2, gPALB2 have similar levels to those found in sporadic tumors. (B, C) Association of the FIS profile signature with tumor size (B) and Gleason score (C) from 497 primary tumors of the The Cancer Genome Atlas data set. Smaller tumors and of lower Gleason score had higher FIS profiles scores. (D, E) Association of the FIS profile signature with the Gleason score (D) and the development of metastasis after radical prostatectomy (E) from 545 samples of the Erho *et al* cohort. (F, G) Kaplan-Meier curve of time to metastasis in the Erho *et al* cohort of 545 patients (F) and the Spratt *et al* cohort of 855 patients (G). Patient tumors with a FIS profile signature above the median had longer times to metastasis. (H) Time to biochemical recurrence in the data set of 73 non-indolent primary prostate cancers from Fraser *et al* showing that the time to biochemical recurrence was longer for tumors with a stronger FIS profile signature. FIS, free immune spatial; *g,* germline; HRD, homologous recombination repair deficiency.

more aggressive disease.[41] One potential hypothesis is that a FIS profile can emerge from distinct underlying biological processes, and these may be distinct in HRD and sporadic tumors. For example, we have shown that the FIS is consistent across grade groups in HRD tumors, whereas it decreases with increasing grade group in sporadic tumors.

While we identified TLS in both the HRD and sporadic cohort, the densities of B cells and TLS were substantially lower than that of T cells and T cell clusters. TLS have been associated with better response to immunotherapy in multiple cancers, including melanoma,[20 21] renal cell carcinoma,[20] head and neck,[42] although this has not been described for PCa. In the KEYNOTE-199 and Checkmate 650 trials, HRD was associated with higher and more durable responses to ICI.[9 39] We did not find enrichment of TLS in the tumor area of the HRD cohort compared with the sporadic cohort, although there was higher

density of B cells in the stroma of HRD samples, thereby accounting for the increased B cell markers seen in the gene expression data for the HRD cohort.

A major unanswered question is the role of the TIME in HRD cancers in mediating durable responses to PARP inhibitors and/or ICIs. Exploratory assays such as FIS profile may complement established genomic assays and warrants further investigation in the context of prospective trials of ICI.

We acknowledge several inherent limitations of our study. We have only analyzed gHRD mutations and have not evaluated somatic events in HRR genes that may also impact the TIME. Recent reports suggest that most germline *BRCA2* events have corresponding heterozygous loss of the second allele.[4] Second, there were only five *BRCA1* cases and one case each of *ATM, CHEK2, PALB2, FANCI,* and *MSH2,* making it impossible to draw definitive conclusions in these smaller subsets. Our findings

should be considered hypothesis-generating and should be further validated in larger prospective studies.

CONCLUSIONS

HRD tumors have a more inflamed TIME than sporadic tumors. A free spatial profile of CD8^{+} T cells may be linked with better disease control. Spatial profiling and the FIS profile signature also provides prognostic information that warrants further investigation in prospective studies.

Author affiliations
[1]Division of Cancer Research, Peter MacCallum Cancer Centre, Melbourne, Victoria, Australia
[2]Sir Peter MacCallum Department of Oncology, The University of Melbourne, Parkville, Victoria, Australia
[3]Department of Medical Oncology, Peter MacCallum Cancer Centre, Melbourne, Victoria, Australia
[4]Institute of Cancer Research Sutton, Sutton, UK
[5]Royal Marsden Hospital Sutton, Sutton, UK
[6]Department of Pathology, Peter MacCallum Cancer Centre, Melbourne, Victoria, Australia
[7]TissuPath, Melbourne, Victoria, Australia
[8]Veracyte Inc, South San Francisco, California, USA
[9]Division of Cancer Surgery, Peter MacCallum Cancer Centre, Melbourne, Victoria, Australia
[10]Austin Hospital, Heidelberg, Victoria, Australia
[11]Division of Radiation Oncology and Cancer Imaging, Peter MacCallum Cancer Centre, Melbourne, Victoria, Australia
[12]Instituto de Investigacion Biomedica de Malaga, Malaga, Spain
[13]Medical Oncology Department, Instituto de Investigación Hospital 12 de Octubre, Madrid, Spain

Twitter Anna Sofia Trigos @anna_t_g

ORCID iDs
Anna Sofia Trigos http://orcid.org/0000-0002-5915-2952
Simon Keam http://orcid.org/0000-0001-9053-9138
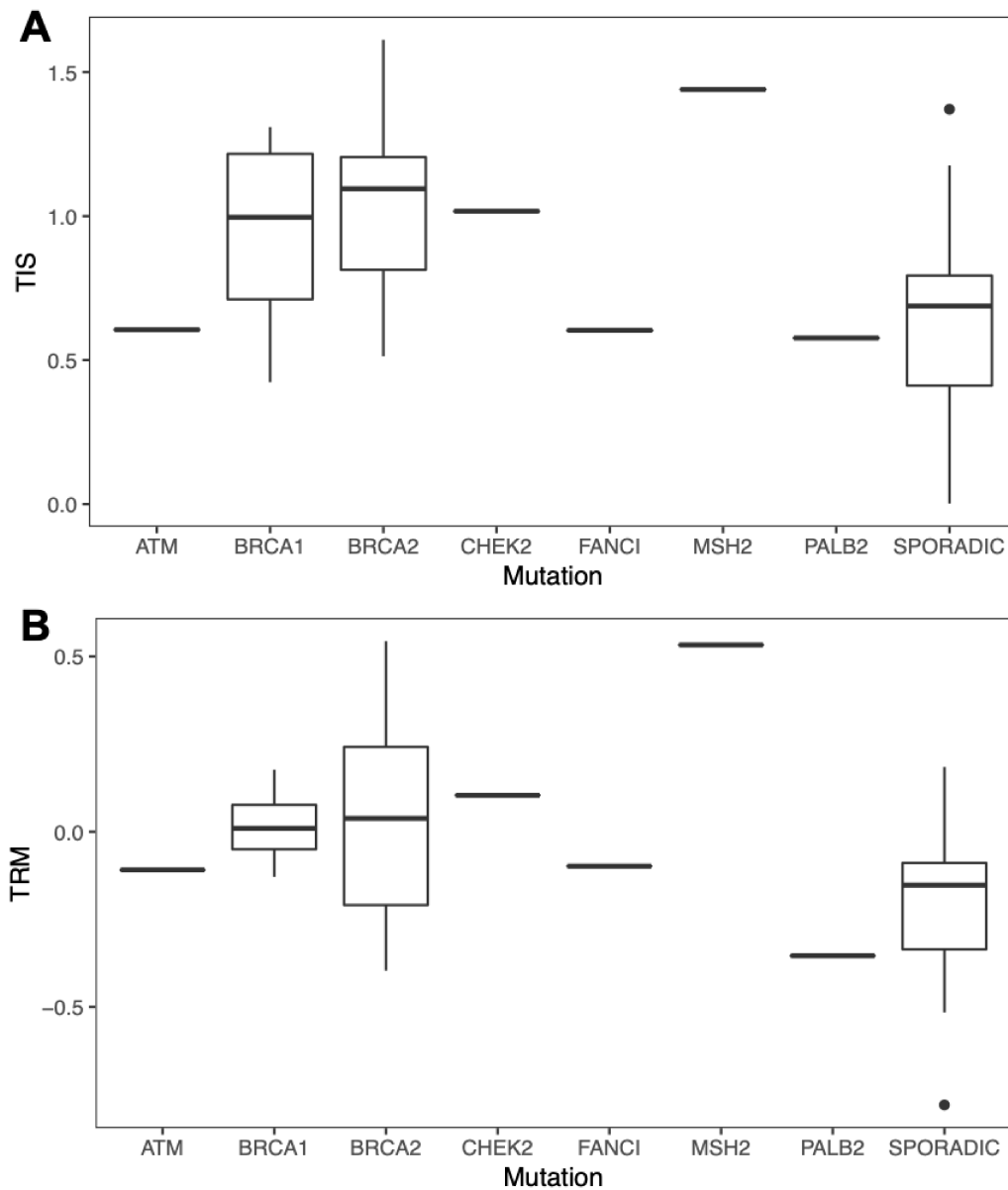Paul Neeson http://orcid.org/0000-0002-2729-5887

REFERENCES
1 de Bono J, Mateo J, Fizazi K, *et al*. Olaparib for metastatic castration-resistant prostate cancer. *N Engl J Med* 2020;382:2091–102.
2 Mateo J, Porta N, Bianchini D, *et al*. Olaparib in patients with metastatic castration-resistant prostate cancer with DNA repair gene aberrations (TOPARP-B): a multicentre, open-label, randomised, phase 2 trial. *Lancet Oncol* 2020;21:162–74.
3 Smith MR, Scher HI, Sandhu S, *et al*. Niraparib in patients with metastatic castration-resistant prostate cancer and DNA repair gene defects (GALAHAD): a multicentre, open-label, phase 2 trial. *Lancet Oncol* 2022;23:362–73.
4 Carreira S, Porta N, Arce-Gallego S, *et al*. Biomarkers associating with PARP inhibitor benefit in prostate cancer in the TOPARP-B trial. *Cancer Discov* 2021;11:2812–27.
5 Clarke B, Tinker AV, Lee C-H, *et al*. Intraepithelial T cells and prognosis in ovarian carcinoma: novel associations with stage, tumor type, and BRCA1 loss. *Mod Pathol* 2009;22:393–402.
6 McAlpine JN, Porter H, Köbel M, *et al*. BRCA1 and BRCA2 mutations correlate with TP53 abnormalities and presence of immune cell infiltrates in ovarian high-grade serous carcinoma. *Mod Pathol* 2012;25:740–50.
7 Nolan E, Savas P, Policheni AN, *et al*. Combined immune checkpoint blockade as a therapeutic strategy for *BRCA1*-mutated breast cancer. *Sci Transl Med* 2017;9:eaal4922.
8 Strickland KC, Howitt BE, Shukla SA, *et al*. Association and prognostic significance of BRCA1/2-mutation status with neoantigen load, number of tumor-infiltrating lymphocytes and expression of PD-1/PD-L1 in high grade serous ovarian cancer. *Oncotarget* 2016;7:13587–98.
9 Antonarakis ES, Piulats JM, Gross-Goupil M, *et al*. Pembrolizumab for treatment-refractory metastatic castration-resistant prostate cancer: Multicohort, open-label phase II KEYNOTE-199 study. *J Clin Oncol* 2020;38:395–405.
10 Sharma P, Pachynski RK, Narayan V, *et al*. Nivolumab plus ipilimumab for metastatic castration-resistant prostate cancer: preliminary analysis of patients in the CheckMate 650 trial. *Cancer Cell* 2020;38:489–99.
11 Berger MF, Lawrence MS, Demichelis F, *et al*. The genomic complexity of primary human prostate cancer. *Nature* 2011;470:214–20.
12 Fridman WH, Zitvogel L, Sautès-Fridman C, *et al*. The immune contexture in cancer prognosis and treatment. *Nat Rev Clin Oncol* 2017;14:717–34.
13 Yang Y, Attwood K, Versaggi C, *et al*. Association of high CD8+ tumor infiltrating lymphocytes at prostatectomy with improved survival of prostate cancer patients. *JCO* 2018;36:5068–68.
14 Nardone V, Botta C, Caraglia M, *et al*. Tumor infiltrating T lymphocytes expressing FoxP3, CCR7 or PD-1 predict the outcome of prostate cancer patients subjected to salvage radiotherapy after biochemical relapse. *Cancer Biol Ther* 2016;17:1213–20.
15 Kärjä V, Aaltomaa S, Lipponen P, *et al*. Tumour-infiltrating lymphocytes: a prognostic factor of PSA-free survival in patients with local prostate carcinoma treated by radical prostatectomy. *Anticancer Res* 2005;25:4435–8.
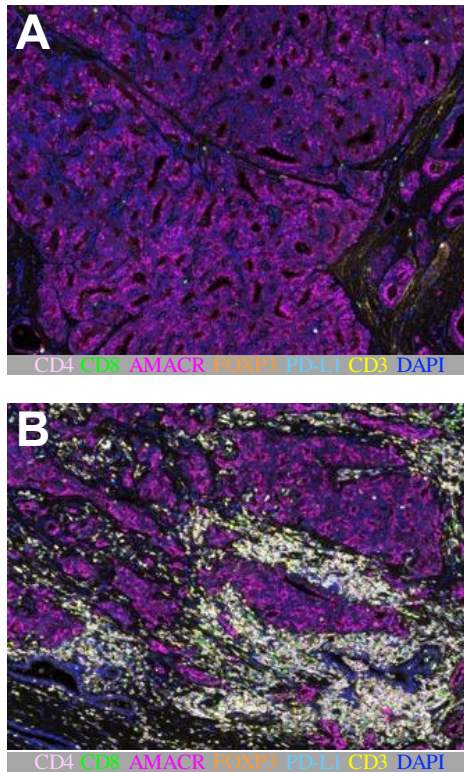
16 Ness N, Andersen S, Valkov A, *et al*. Infiltration of CD8+ lymphocytes is an independent prognostic factor of biochemical failure-free survival in prostate cancer. *Prostate* 2014;74:1452–61.

17 Leclerc BG, Charlebois R, Chouinard G, *et al*. CD73 expression is an independent prognostic factor in prostate cancer. *Clin Cancer Res* 2016;22:158–66.

18 Petitprez F, Fossati N, Vano Y, *et al*. PD-L1 expression and CD8+ T-cell infiltrate are associated with clinical progression in patients with node-positive prostate cancer. *Eur Urol Focus* 2019;5:192–6.

19 Zhao SG, Lehrer J, Chang SL, *et al*. The immune landscape of prostate cancer and nomination of PD-L2 as a potential therapeutic target. *J Natl Cancer Inst* 2019;111:301–10.

20 Helmink BA, Reddy SM, Gao J, *et al*. B cells and tertiary lymphoid structures promote immunotherapy response. *Nature* 2020;577:549–55.

21 Cabrita R, Lauss M, Sanna A, *et al*. Tertiary lymphoid structures improve immunotherapy and survival in melanoma. *Nature* 2020;577:561–5.

22 Petitprez F, de Reyniès A, Keung EZ, *et al*. B cells are associated with survival and immunotherapy response in sarcoma. *Nature* 2020;577:556–60.

23 Keren L, Bosse M, Marquez D, *et al*. A structured tumor-immune microenvironment in triple negative breast cancer revealed by multiplexed ion beam imaging. *Cell* 2018;174:e19:1373–87.

24 Huang Y-K, Wang M, Sun Y, *et al*. Macrophage spatial heterogeneity in gastric cancer defined by multiplex immunohistochemistry. *Nat Commun* 2019;10:3928.

25 Saltz J, Gupta R, Hou L, *et al*. Spatial organization and molecular correlation of tumor-infiltrating lymphocytes using deep learning on pathology images. *Cell Rep* 2018;23:181–93.

26 Gong C, Anders RA, Zhu Q, *et al*. Quantitative characterization of CD8+ T cell clustering and spatial heterogeneity in solid tumors. *Front Oncol* 2018;8:649.

27 Ayers M, Lunceford J, Nebozhyn M, *et al*. IFN-γ-related mRNA profile predicts clinical response to PD-1 blockade. *J Clin Invest* 2017;127:2930–40.

28 Savas P, Virassamy B, Ye C, *et al*. Single-cell profiling of breast cancer T cells reveals a tissue-resident memory subset associated with improved prognosis. *Nat Med* 2018;24:986–93.

29 Yang T, Ozcoban V, Pasam A. SPIAT: an R package for the spatial image analysis of cells in tissues. *bioRxiv* 2020.

30 Cancer Genome Atlas Research Network. The molecular taxonomy of primary prostate cancer. *Cell* 2015;163:1011–25.

31 Fraser M, Sabelnykova VY, Yamaguchi TN, *et al*. Genomic hallmarks of localized, non-indolent prostate cancer. *Nature* 2017;541:359–64.

32 Ben-Salem S, Hu Q, Liu Y, *et al*. Diversity in androgen receptor action among treatment-naïve prostate cancers is reflected in treatment response predictions and molecular subtypes. *Eur Urol Open Sci* 2020;22:34–44.

33 Spratt DE, Yousefi K, Deheshi S, *et al*. Individual patient-level meta-analysis of the performance of the decipher genomic classifier in high-risk men after prostatectomy to predict development of metastatic disease. *J Clin Oncol* 2017;35:1991–8.

34 Erho N, Crisan A, Vergara IA, *et al*. Discovery and validation of a prostate cancer genomic classifier that predicts early metastasis following radical prostatectomy. *PLoS One* 2013;8:e66855.

35 Edwards J, Wilmott JS, Madore J, *et al*. CD103+ tumor-resident CD8+ T cells are associated with improved survival in immunotherapy-naïve melanoma patients and expand significantly during anti-PD-1 treatment. *Clin Cancer Res* 2018;24:3036–45.

36 Guedes LB, Antonarakis ES, Schweizer MT, *et al*. MSH2 loss in primary prostate cancer. *Clin Cancer Res* 2017;23:6863–74.

37 Haffner MC, Guner G, Taheri D, *et al*. Comprehensive evaluation of programmed death-ligand 1 expression in primary and metastatic prostate cancer. *Am J Pathol* 2018;188:1478–85.

38 Glinsky GV, Glinskii AB, Stephenson AJ, *et al*. Gene expression profiling predicts clinical outcome of prostate cancer. *J Clin Invest* 2004;113:913–23.

39 Initial results from a phase II study of nivolumab (NIVO) plus ipilimumab (IPI) for the treatment of metastatic castration-resistant prostate cancer (mCRPC; CheckMate 650). Genitourinary Cancers Symposium; 2019 Presented February 14, 2019; San Francisco, CA.

40 Jenzer M, Keß P, Nientiedt C, *et al*. The BRCA2 mutation status shapes the immune phenotype of prostate cancer. *Cancer Immunol Immunother* 2019;68:1621–33.

41 Pritchard CC, Mateo J, Walsh MF, *et al*. Inherited DNA-repair gene mutations in men with metastatic prostate cancer. *N Engl J Med* 2016;375:443–53.

42 Ruffin AT, Cillo AR, Tabib T, *et al*. B cell signatures and tertiary lymphoid structures contribute to outcome in head and neck squamous cell carcinoma. *Nat Commun* 2021;12:3349.

Supplemental material

BMJ Publishing Group Limited (BMJ) disclaims all liability and responsibility arising from any reliance
placed on this supplemental material which has been supplied by the author(s)

J Immunother Cancer

Supplementary Figures

Supplementary Figure S1. TIS and TRM signature levels by germline mutation status.

(A) TIS levels. HRD tumors have higher TIS levels compared to sporadic tumors. **(B)** TRM signature levels. HRD tumors have higher TRM signature levels compared to sporadic tumors.

Supplemental material

BMJ Publishing Group Limited (BMJ) disclaims all liability and responsibility arising from any reliance placed on this supplemental material which has been supplied by the author(s)

J Immunother Cancer

Supplementary Figure S2. T-cell microenvironment in sporadic tumors.

mIHCs showing the heterogeneity of T cells in the tumor area of primary prostate cancer, which ranges from immune deserts **(A)** to high levels of T-cell infiltration **(B)**.

Supplemental material

BMJ Publishing Group Limited (BMJ) disclaims all liability and responsibility arising from any reliance placed on this supplemental material which has been supplied by the author(s)

J Immunother Cancer
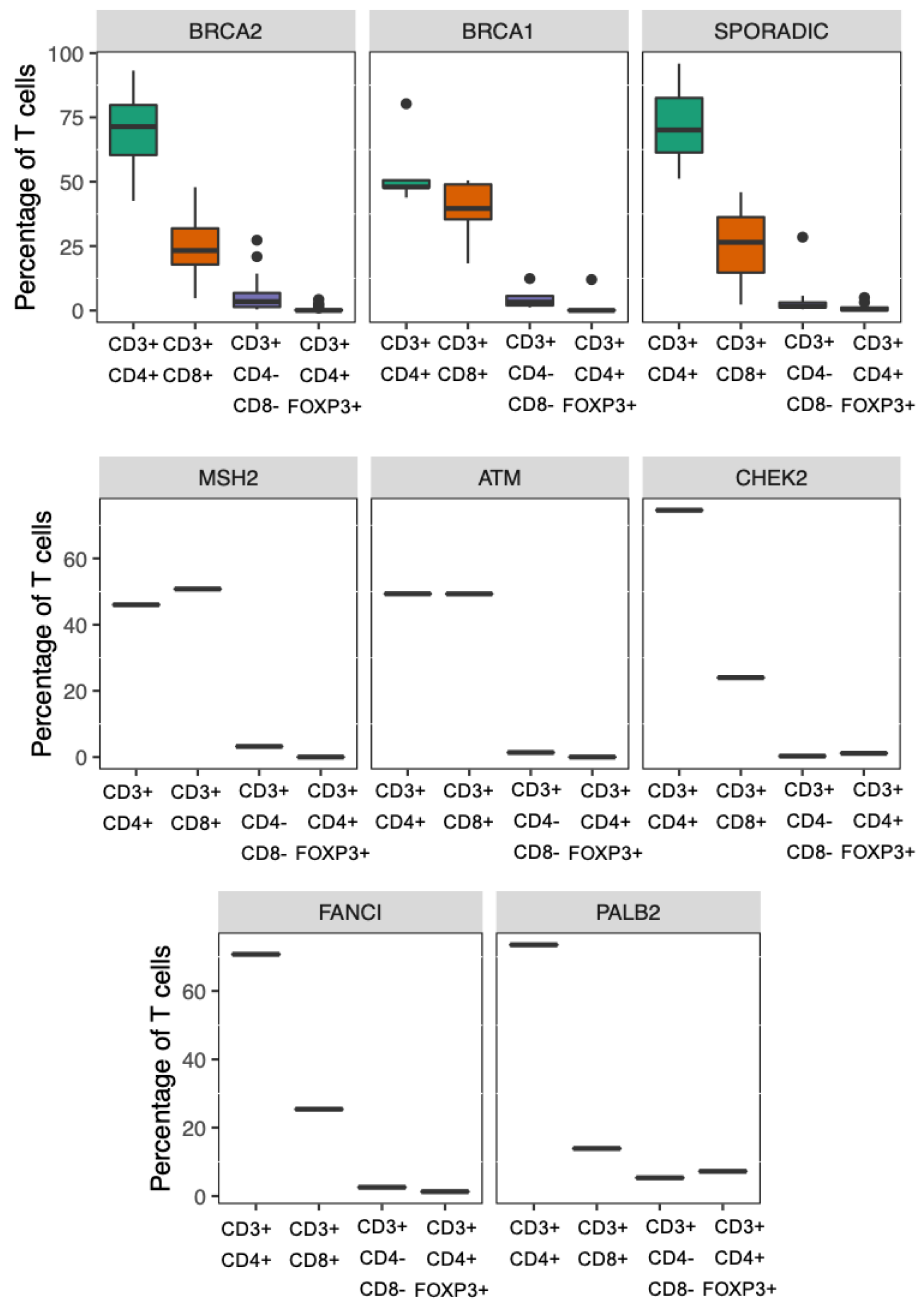
Supplementary Figure S3. T-cell populations in the TIME of HRD and sporadic tumors.
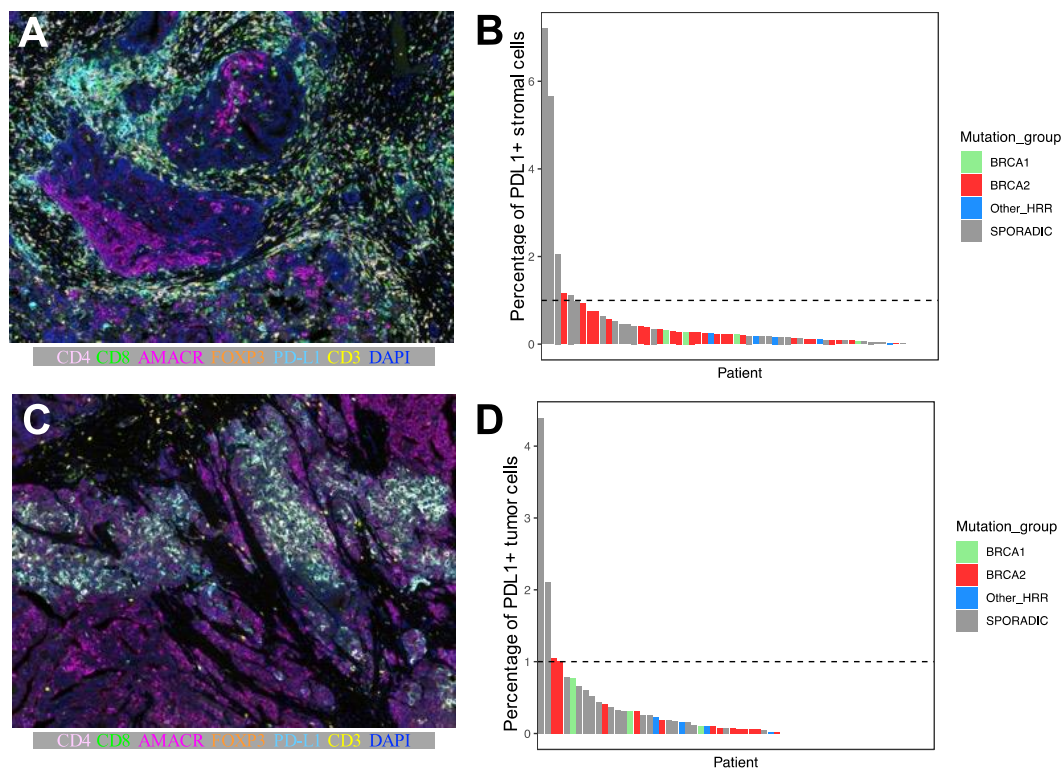
Supplementary Figure S4. PDL1+ cells in the TIME of primary prostate cancer.

(A) mIHC showing a tumor area with high levels of PDL1+ stromal cells adjacent to tumor cells. **(B)** Distribution of percentages of PDL1+ stromal cells across the cohort. Most tumors had less than 1% or no PDL1+ stromal cells. Stromal cells were defined as (CD3+CD4+, CD3+CD8+, CD3+CD4-CD8-, CD3+CD4+FOXP3+ or PDL1+). **(C)** mIHC showing a tumor area with high levels of PDL1+ tumor cells. Although PDL1+ tumor cells were rare, patches were observed across the cohort. **(D)** Distribution of percentages of PDL1+ tumor cells across the cohort. Most tumors had less than 1% or no PDL1+ tumor cells.

mIHC colors: pink (CD4), green (CD8), magenta (AMACR), orange (FOXP3), cyan (PDL1), yellow (CD3), dark blue (DAPI).
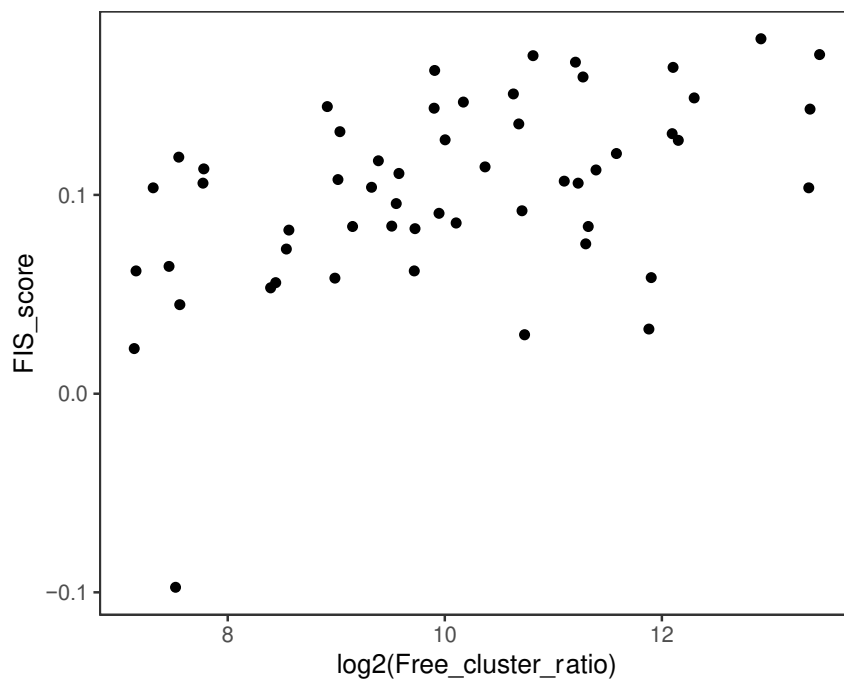
Supplementary Figure S5. Association between FIS profile signature and the ratio of free/clustered T cells. Spearman correlation = 0.45, p-value=4.07×10^{-4}.
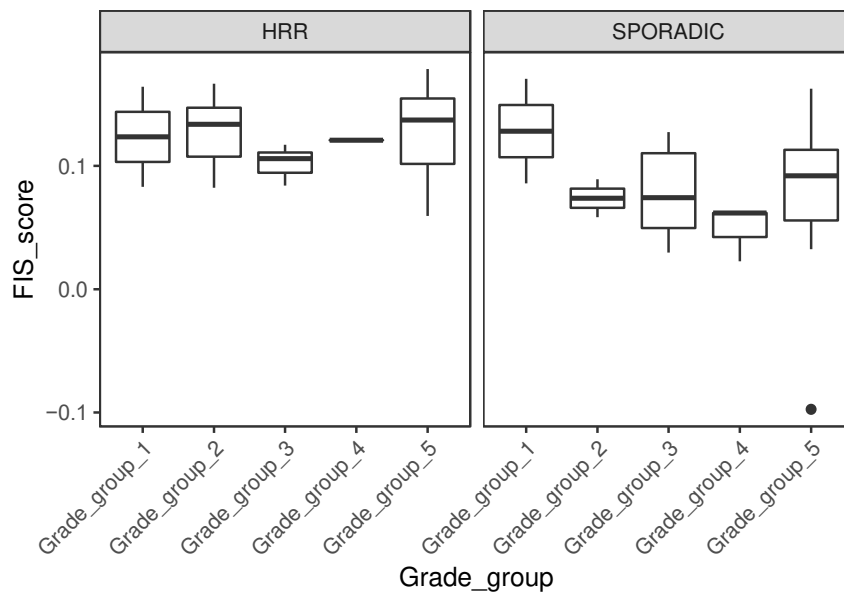
Supplementary Figure S6. FIS scores across Grade groups in the HRR and sporadic cohorts. Sporadic samples have lower FIS scores than HRR samples in Grade groups 2-5. There is a decreasing trend in sporadic tumors, although this is not significant (Jonckheere-Terpstra test=0.42).
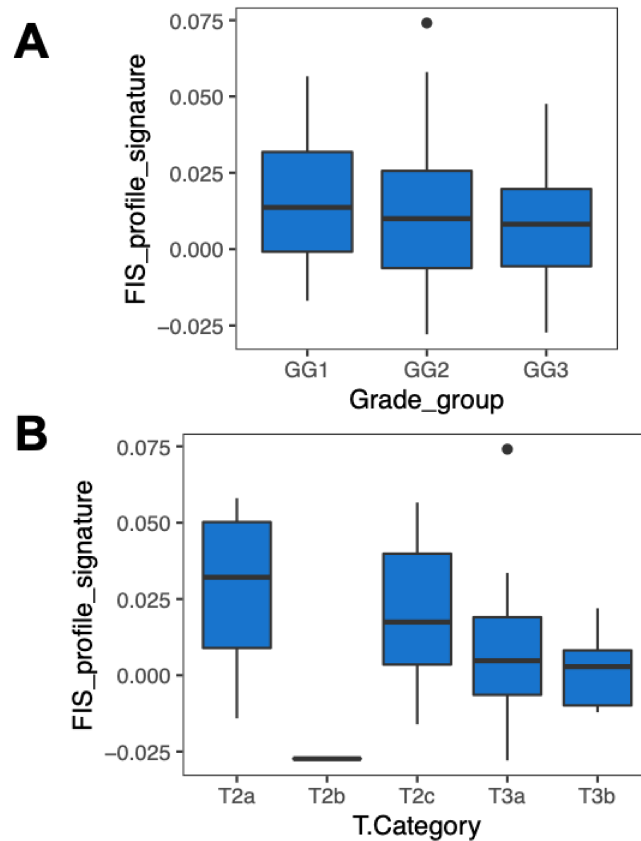
Supplementary Figure S7. Association between grade group and tumor size with FIS profile scores in the dataset by Fraser et al.

(A) Higher grade group tumors tended to have lower levels of the FIS profile signature, although the trend was not significant (Jonckheere-Terpstra p-value = 0.31). **(B)** Larger tumors tended to have lower levels of the FIS signature, consistent with poor immune control (p-value = 0.0027).
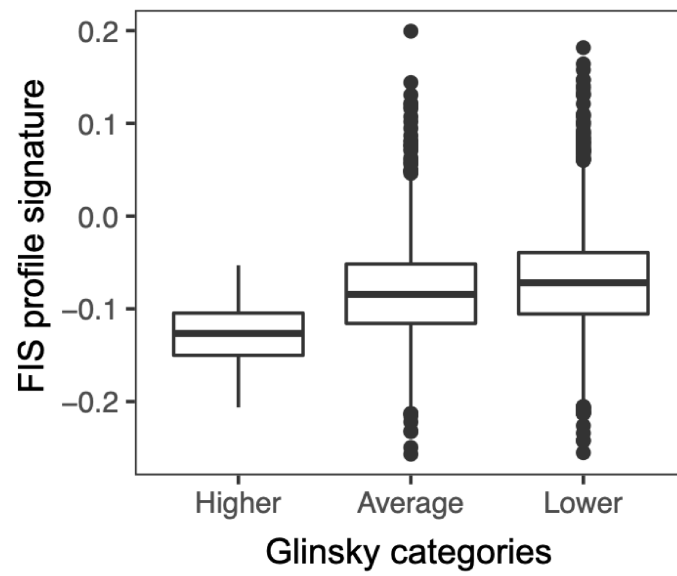
Supplementary Figure S8. FIS profile signature levels according to Glinsky et al., signature score risk groups in a cohort of 8,635 prostate cancer samples from the GRID database.

Lower Glinsky signature scores are associated with better prognosis and higher levels of the FIS profile signature (Jonckheere-Terpstra p-value $< 2 \times 10^{-4}$). (Higher n=136, average n=2,591 and lower n=5,908, total n=8,635).

Supplementary Methods

Identification of germline mutations in HRR genes

Confirmation of a participant's germline mutation status was performed using a variety of sequencing platforms at the Peter MacCallum Molecular Pathology NATA accredited clinical laboratory. Variants were assigned a class C4–C5 (pathogenic) mutation status according to a 5-tier clinical classification introduced by ENIGMA http://www.enigmaconsortium.org/. Variants are listed in Table S2.

Differential expression and normalization

We used the RUV R package (Removal of Unwanted Variation)[1,2] for normalization and differential gene expression analysis. For differential expression analysis we used RUV-4, with genes annotated as housekeeping, positive control and negative control genes by Nanostring as control genes. We chose a *k* that resulted in a uniform distribution of empirical p-values. Resulting nominal p-values were adjusted using the Benjamini & Hochberg method. Genes with an adjusted p-value less than 0.05 and were considered to be significant. For normalization, we used RUVIII. We extended our set of control genes used for differential expression analysis with RUV-4 to also include genes that showed no signal of differential expression (adjusted p-value > 0.5 and absolute log2 fold change less than 0.3).

Tumor inflammation signature (TIS)

We used the following 16 genes to perform TIS[3] analyses: *CXCR6*, *TIGIT*, *CD27*, *CD274*, *PDCD1LG2*, *LAG3*, *PSMB10*, *CMKLR1*, *CD8A*, *IDO1*, *CCL5*, *CXCL9*, *HLA-DQA1*, *CD276*, *STAT1*, *HLA-E*. Two additional genes of the original signature, *NKG7* and *HLA-DRB1*, were not present in the Nanostring PanCancer Immune Profiling Panel and were excluded. This reduced TIS signature has been published previously[4]. TIS scores were calculated for individual samples by averaging the normalized gene expression of these genes.

Tissue-resident memory T-cell (TRM)

We used 37 genes from previously published TRM signature of 179 genes[5] that were present in the Nanostring PanCancer Immune Profiling Panel platform. A similar procedure has been previously carried out by other authors[6]. TRM scores were calculated for individual samples by averaging the normalized gene expression of these genes.

Multiplex immunohistochemistry

Sections from formalin-fixed paraffin embedded (FFPE) tumor blocks were stained with H&E and marked by two pathologists for tumor-rich regions. We used a T cell panel with primary antibodies for CD3 (clone SP7 1:500, Abcam), CD4 (clone SP35, 1:100 Abcam), CD8 (clone4B11, 1:500, Leica Biosystems), FOXP3 (1: 200, Bio SB), PD-L1 (clone SP142, 1:500 Abcam), AMACR (13H4 1:1000, Cell Marque) and DAPI for cell visualization and identification, as we have done previously[4,7,8]. Our combination of markers allowed us to distinguish $CD3^+CD4^+$ (helper T cells), $CD3^+CD8^+$ (cytotoxic T cells), $CD3^+CD4^+FOXP3^+$ (regulatory T cells), tumor cells ($AMACR^+$) and $PD-L1^+$ cells.

Slides (4uM sections) were baked at 60^oC, dewaxed prior to antigen retrieval followed by primary antibody for 30min and 0.3% H_2O_2 block for 10min at room temperature (RT). Anti-rabbit or Anti-mouse HRP-conjugated secondary antibody from Perkin Elmer (1:500 dilution) was applied for 10min at RT. Signal amplification was carried out using TSA Plus (1:100 in TSA amplification diluent, PerkinElmer) for 10min. Three (2min each) washes were performed in between each step using TBST (0.05% Tween-20). Slides were microwaved as per PerkinElmer instructions to strip the primary-secondary-HRP complex allowing introduction of the next antibody. After the final antibody, the slides were incubated with DAPI for 1 min and coverslips were placed with mounting medium. Single antibody

4

controls were included with each antibody. Visualization of the seven-color OPAL slides was performed using Perkin Elmer's Vectra 3.0 automated imaging system. Tissue segmentation, cell segmentation and phenotyping of images was performed using the inForm Advanced Image Analysis Software (versions 2.3 and 2.4). We took 15 representative multispectral images of 1.34 mm^2 of the tumor area identified by a pathologist. Cell types were quantified in each image, and then averaged per tumor sample. The density of T cells was calculated as the ratio of the number of T cells in an image and the image size (1.34 mm^2). The field resolution was 20x (0.5μm) with an image size of 1338 μm x 1004 μm.

Deriving the FIS signature

We derived gene expression signatures for the FIS profile by calculating the Spearman correlation between the ratio of free and clustered CD8+ cells and the genes available in the Nanostring platform and selecting the top 5 genes, which had a positive Spearman correlation greater than 0.25 and p-values < 0.05. Signature levels were measured using *singscore*[9].

5

References

1. Molania R, Gagnon-Bartsch JA, Dobrovic A, Speed TP. A new normalization for Nanostring nCounter gene expression data. *Nucleic Acids Res.* 2019;47(12):6073-6083.
2. Gagnon-Bartsch JA, Speed TP. Using control genes to correct for unwanted variation in microarray data. *Biostatistics.* 2012;13(3):539-552.
3. Ayers M, Lunceford J, Nebozhyn M, et al. IFN-gamma-related mRNA profile predicts clinical response to PD-1 blockade. *J Clin Invest.* 2017;127(8):2930-2940.
4. Keam SP, Halse H, Nguyen T, et al. High dose-rate brachytherapy of localized prostate cancer converts tumors from cold to hot. *J Immunother Cancer.* 2020;8(1).
5. Savas P, Virassamy B, Ye C, et al. Single-cell profiling of breast cancer T cells reveals a tissue-resident memory subset associated with improved prognosis. *Nature Medicine.* 2018;24(7):986-993.
6. Solomon B, Young RJ, Bressel M, et al. Identification of an excellent prognosis subset of human papillomavirus-associated oropharyngeal cancer patients by quantification of intratumoral CD103+ immune cell abundance. *Ann Oncol.* 2019;30(10):1638-1646.
7. Wang M, Huang Y-K, Kong JC, et al. High-dimensional analyses reveal a distinct role of T-cell subsets in the immune microenvironment of gastric cancer. *Clinical & translational immunology.* 2020;9(5):e1127-e1127.
8. Halse H, Colebatch AJ, Petrone P, et al. Multiplex immunohistochemistry accurately defines the immune context of metastatic melanoma. *Sci Rep.* 2018;8(1):11158.
9. Foroutan M, Bhuva DD, Lyu R, Horan K, Cursons J, Davis MJ. Single sample scoring of molecular phenotypes. *BMC Bioinformatics.* 2018;19(1):404.

Supplemental material

BMJ Publishing Group Limited (BMJ) disclaims all liability and responsibility arising from any reliance placed on this supplemental material which has been supplied by the author(s)

J Immunother Cancer

Supplementary Tables

Supplemental material

BMJ Publishing Group Limited (BMJ) disclaims all liability and responsibility arising from any reliance placed on this supplemental material which has been supplied by the author(s)

J Immunother Cancer

Table S1. Clinical characteristics of cohort

	Sporadics	gBRCA2	gBRCA1	gATM	gCHEK2	gFANCI	gMSH2+ gBRCA2	gPALB2
Patients (N)	26	26	5	1	1	1	1	1
Age at diagnosis (Mean)	61.5 (47-78)	61.96 (39-77)	63 (59-69)	55	67	70	57	53
PSA at diagnosis (Mean)	13.07 (2.0-56.0)	10.75 (1.9-65.3)	14.6 (2.0-49.1)	5	7.7	6500	8.8	4.3
Grade group 1 (N)	2	2						
Grade group 2 (N)	2	7	1				1	
Grade group 3 (N)	6	5	2		1			
Grade group 4 (N)	3	1						
Grade group 5 (N)	13	11	2	1		1		1

Table S2: Variants of germline mutations

Sample ID	Mutation	Variant	Pathogenicity
Pt 1	*gBRCA1*	BRCA1 c.5095 C>T pArg1699Trp in exon 18	C5
Pt 2	*gBRCA1*	BRCA1 c.2071 del A	C5
Pt 3	*gBRCA1*	BRCA1 917_918 del TT (STOP 285)	C5
Pt 4	*gBRCA1*	BRCA1 c.135-1G>T	C5
Pt 5	*gBRCA1*	BRCA1 c135-1G>T	C5
Pt 6	*gBRCA2*	BRCA2 6174 del T in exon 11	C5
Pt 7	*gBRCA2*	BRCA2 IVS 17-1 G>C	C5
Pt 8	*gBRCA2*	BRCA2 542 T>G (L105X)	C5
Pt 9	*gBRCA2*	BRCA2 c.8585dupT; p.Glu2863Argfs*6 exon 20	C5
Pt 10	*gBRCA2*	BRCA2 5910 C>G (Y1894X)	C5
Pt 11	*gBRCA2*	BRCA2 2041_2042 del A (STOP 613)	C5
Pt 12	*gBRCA2*	BRCA2 c.6275_6276delTT; p.Leu2092Profs*7 exon 11	C5
Pt 13	*gBRCA2*	BRCA2 c.2760delC; p.Ile921PhefsX39 in exon 11	C5
Pt 14	*gBRCA2*	BRCA2 c.7480C>T; p.Arg2494* in exon 15	C5
Pt 15	*gBRCA2*	BRCA2 c.5682C>G; p.Tyr1894* in exon 11	C5
Pt 16	*gBRCA2*	BRCA2 c.1813delA; p.lie605Tyrfs* in exon 10	C5
Pt 17	*gBRCA2*	BRCA2 c.4211C>G; p.Ser1404*	C5
Pt 18	*gBRCA2*	BRCA2 978_983del4 in exon 9	C5
Pt 19	*gBRCA2*	BRCA2 2041_2042 del A (STOP 613)	C5
Pt 20	*gBRCA2*	BRCA2 c.5279C>G: p.Ser1760X in exon 11	C5
Pt 21	*gBRCA2*	BRCA2 9117 G>A (P3039P)	C5
Pt 22	*gBRCA2*	BRCA2 7985G>A	C5
Pt 23	*gBRCA2*	BRCA2 c.9097dupA; p.Thr3033Asnfs*11 exon 23	C5
Pt 24	*gBRCA2*	BRCA2 9132 del C (STOP 2975)	C5
Pt 25	*gBRCA2*	BRCA2 c.778_779delGA: p.Glu260Serfs*15 exon 9	C5
Pt 26	*gBRCA2*	BRCA2 c.5073dupA p.Trp1692MetfsTer3	C5
Pt 27	*gBRCA2*	BRCA2 9522 C>G (Y3098X)	C5
Pt 28	*gBRCA2*	BRCA2 983delACAG exon 9	C5
Pt 29	*gBRCA2*	BRCA2 9345 G>A (splice variant)	C5
Pt 30	*gBRCA2*	BRCA2 c.771_775delTCAAA; p.Asn257Lysfs*17 exon 9	C5
Pt 31	*gBRCA2*	BRCA2 c.68-?_6841+?del	C5

Pt 32	*gMSH2+gBRCA2*	BRCA2 c.517-2A in intron 6 and MSH2 Deletion of exon 8	C5 (*MSH2*) and C4 (*BRCA2*)
Pt 33	*gCHEK2*	c.320-5T>A	C4
Pt 34	*gFANCI*	c.511C>T	C5
Pt 35	*gPALB2*	c.2368C>T	C5
Pt 36	*gATM*	c.7829_7830del	C5

Table S3: Differentially expressed genes between HRR and sporadic samples.
A positive log fold change (logFC) indicates upregulation in the HRR samples.

Gene	logFC	p-value	Adjusted p-value
CCL25	-0.6447166	9.54E-03	0.04131796
CD1D	0.76410547	1.82E-05	0.0003853
FPR2	-1.1590316	8.74E-06	0.0002076
IL5	-0.9124614	1.65E-03	0.01164058
IKBKE	0.65063944	2.71E-03	0.01600989
INPP5D	0.70148955	1.28E-06	5.59E-05
CD53	0.66022119	2.86E-06	9.74E-05
CTSG	-1.1592962	9.65E-05	0.00135076
LTB	1.13620959	1.63E-05	0.00035522
CCL28	0.9968652	1.82E-03	0.01221736
CARD11	0.85893254	5.01E-06	0.00013541
SPN	0.66862197	1.88E-04	0.00227019
PRF1	0.47406432	4.17E-04	0.00413459
CCL26	-0.8102846	1.62E-04	0.00201249
CCL15	-0.8678269	5.51E-04	0.00501949
TNFSF10	0.8393136	1.15E-04	0.00150524
TLR6	0.60338788	3.34E-04	0.00367032
S100B	-1.1180312	5.98E-06	0.00015622
TLR10	0.79949463	8.57E-05	0.00125549
CD22	0.64550198	3.99E-03	0.02158515
CD209	-0.5871911	5.97E-03	0.02891531
KLRG1	0.67286043	4.86E-04	0.00453528
CXCR2	-0.8607383	3.67E-04	0.00383947
MAGEA1	-0.8063779	4.82E-03	0.02501223
CD36	-1.169591	8.28E-06	0.00020292
CXCR3	1.03951576	1.47E-08	1.32E-06
TLR1	0.7277777	3.34E-07	1.74E-05
IL1R2	-0.8248538	8.20E-04	0.00677105
PTPRC	0.80733115	9.93E-09	1.30E-06
APOE	0.83263548	6.84E-03	0.03136965
LY9	0.65223803	1.03E-03	0.00803614
HLA-DMB	1.09759019	6.43E-04	0.00549292
FCER1G	0.41530016	3.22E-03	0.01841075
CD40	0.378842	6.15E-03	0.02959895
CASP1	0.40231718	6.78E-03	0.0312727
ITGAX	0.46918834	2.14E-03	0.01363641
CCL19	0.96855437	2.16E-03	0.01363641

PTGS2	-1.3062756	3.51E-04	0.00374182
CD27	0.79646604	8.43E-05	0.00125549
PSMB10	0.3641815	6.78E-03	0.0312727
PSMB8	0.58272919	1.29E-03	0.00969337
HLA-A	1.37660257	4.67E-11	3.66E-08
SLAMF7	0.70378776	1.15E-03	0.00890917
IL6	-2.3171993	1.08E-06	4.97E-05
IL21R	0.53395163	5.75E-03	0.02863919
CD3G	0.65156577	1.78E-03	0.01213017
VEGFC	-0.3526383	6.51E-03	0.03057212
IL2RG	0.97824948	5.65E-10	1.32E-07
C3	0.99426956	9.87E-05	0.00135786
PRG2	-0.7714846	1.68E-03	0.01164058
IL1R1	-0.6743912	3.90E-03	0.02138804
CD96	1.06576974	6.73E-10	1.32E-07
GZMK	0.7440735	1.70E-03	0.01169581
CYBB	0.69567433	6.23E-08	4.07E-06
HLA-DOB	0.6883734	4.39E-04	0.00424737
NOD2	0.47675574	2.01E-03	0.01314212
SYK	0.74392358	3.19E-04	0.00357288
PIK3CD	0.7697434	1.84E-06	6.89E-05
CASP8	0.5272876	1.36E-03	0.01006645
CMKLR1	0.35875128	3.87E-03	0.02138723
HLA-DRA	0.78770694	3.15E-04	0.00357288
IL16	0.65477757	9.21E-06	0.00021243
GTF3C1	-0.4977002	6.30E-03	0.02994698
SH2D1A	0.78018479	4.88E-05	0.0008411
CMA1	-0.9773325	1.53E-03	0.01108815
TNFRSF13B	0.81029717	6.24E-03	0.02983897
CD58	0.67750057	4.90E-06	0.00013541
CD6	0.47345671	2.72E-03	0.01600989
KLRK1	0.87998976	3.82E-05	0.00067979
TLR7	0.63338636	3.07E-04	0.00353862
IRF1	0.65901675	1.50E-03	0.01096402
NFKBIA	-0.3342822	9.34E-04	0.00747277
CLEC4C	0.70027323	1.02E-02	0.04257253
IL22	-0.7653724	5.92E-04	0.00527721
NEFL	-1.1387951	6.75E-03	0.0312727
IL32	0.70561418	6.25E-06	0.00015817
IRF8	0.59716456	1.13E-04	0.00150049
NT5E	-0.485135	4.34E-03	0.02315809
TAL1	-0.5060052	9.88E-03	0.04209206

ICOS	0.52961005	8.00E-03	0.03581009
TNF	0.8876652	1.80E-03	0.01214208
CD180	0.62779565	7.46E-04	0.00629116
C1R	0.56759448	1.54E-03	0.01108815
ATG7	0.35312935	2.24E-03	0.01385269
ITGA4	0.51101712	8.65E-05	0.00125549
CXCL13	1.49997177	1.02E-02	0.04257253
MCAM	-0.6676763	3.72E-04	0.00383947
BTLA	0.81988418	3.53E-04	0.00374182
JAK3	0.54863152	7.29E-05	0.00114369
CD3D	1.13147557	4.91E-10	1.32E-07
ARG1	-1.1440988	1.87E-04	0.00227019
CD247	0.83268811	2.15E-08	1.69E-06
C8B	-0.8824562	4.36E-06	0.00012672
THBD	-0.6702777	5.82E-04	0.00524068
UBC	-0.4072711	5.85E-03	0.02868688
LBP	-0.7929712	7.00E-03	0.03190039
SPANXB1	-0.728331	7.23E-03	0.03278202
ITGAM	0.60873521	3.52E-05	0.00065692
TNFRSF17	1.00886744	1.64E-03	0.01164058
TREM1	-1.4611974	1.67E-03	0.01164058
IFNA8	-0.8822249	5.77E-03	0.02863919
SLC11A1	-0.8986624	1.36E-03	0.01006645
ABL1	-0.3976347	4.37E-04	0.00424737
TIGIT	0.61174755	2.23E-03	0.01385269
TCF7	0.46456448	6.44E-03	0.03042148
CXCL11	1.02009402	4.81E-03	0.02501223
BLK	0.86000239	2.30E-03	0.01395583
CCL5	0.4453199	4.89E-03	0.02505203
CD79A	1.52641399	9.13E-05	0.00130149
CTSH	0.57327396	5.13E-03	0.02613011
ITGAL	1.15685313	1.70E-07	9.53E-06
AMICA1	0.55943575	1.11E-04	0.00150049
IL12RB1	0.45919552	4.74E-03	0.02495711
CX3CR1	1.05877515	4.07E-04	0.00413459
CD34	-0.7084816	8.05E-04	0.00671713
CTAGE1	-0.809441	3.65E-05	0.00066567
SEMG1	-4.6145887	6.06E-04	0.00528853
PSMB9	0.96142368	1.24E-07	7.48E-06
HLA-G	0.84861689	5.00E-05	0.0008411
OSM	-1.0870104	6.45E-04	0.00549292
TNFRSF12A	-1.1058863	2.26E-03	0.01385754

IFNAR2	0.43105011	5.04E-05	0.0008411
C1QB	0.44096031	3.37E-03	0.019022
IFNA7	-0.6614625	4.13E-04	0.00413459
LCK	0.77070067	1.26E-08	1.32E-06
MAPKAPK2	0.39291615	5.30E-03	0.02665665
CD5	0.73861026	3.68E-06	0.00011537
IRF4	0.61626213	8.97E-03	0.03927201
SELE	-1.0268323	3.65E-03	0.02030067
CEACAM8	-0.5103837	8.17E-03	0.03617375
CD79B	1.25592713	2.14E-06	7.64E-05
ZAP70	0.69506213	2.48E-04	0.00289662
HLA-B	0.44554884	4.53E-03	0.02400743
PDGFRB	0.43193063	4.10E-03	0.02202151
CD19	0.93733979	7.26E-05	0.00114369
PASD1	-0.7926381	3.61E-03	0.02023
IL3	-0.5725111	5.95E-03	0.02891531
MME	-1.0487269	1.03E-02	0.04257253
CDKN1A	-0.7789121	9.49E-04	0.00751616
SYCP1	-0.6779428	5.82E-03	0.02868688
NLRC5	0.65062957	3.48E-06	0.00011382
LILRB2	-0.5717309	3.93E-03	0.02138804
FAS	0.6415598	2.09E-03	0.01353227
IL2RB	0.98161871	2.39E-05	0.00046811
IL25	-0.5139503	7.65E-03	0.03447953
MAGEA12	-0.7583705	1.85E-03	0.01227819
IL1RL2	-0.5130586	8.65E-03	0.03810807
STAT4	0.38386429	1.19E-02	0.04895978
LAMP3	1.17939883	2.04E-05	0.00040929
CXCL10	1.12446021	8.56E-04	0.00698742
CCR1	0.54657274	9.96E-03	0.04209206
ITGA6	-0.5071367	3.36E-03	0.019022
ITGB3	-0.7050994	4.59E-04	0.00438913
S100A8	-1.2524339	5.15E-04	0.00475433
CSF1R	0.48264615	2.31E-03	0.01395583
LY86	0.49571349	2.24E-03	0.01385269
CEACAM6	1.19018642	2.71E-03	0.01600989
CXCL9	1.30328179	5.50E-05	0.0008989
IDO1	0.58183069	4.85E-03	0.02503681
CAMP	-1.0084129	2.15E-03	0.01363641
MS4A1	1.5660516	8.20E-05	0.00125549
PIK3CG	0.79089215	3.63E-07	1.78E-05
CTSS	0.65391267	6.07E-04	0.00528853

Supplemental material

BMJ Publishing Group Limited (BMJ) disclaims all liability and responsibility arising from any reliance placed on this supplemental material which has been supplied by the author(s)

J Immunother Cancer

IL27	-0.5753489	8.04E-03	0.03581009
IFNA17	-0.68553	9.99E-03	0.04209206
PSMD7	-0.477481	4.82E-04	0.00453528
CCR5	0.44618618	1.99E-03	0.01313675
S100A12	-1.454304	1.18E-04	0.00151423
IL10RA	0.75049818	1.52E-08	1.32E-06
GZMA	0.81502376	4.13E-06	0.00012461
VEGFA	-1.1444038	8.73E-04	0.00705863
HLA-DPB1	0.91690008	2.80E-09	4.39E-07
CD48	0.64271578	3.46E-05	0.00065692
PRM1	-0.6321258	2.93E-03	0.01703077
PDCD1LG2	0.5586415	1.26E-03	0.00957928
LRP1	0.53110812	1.91E-04	0.00227183
CCR2	0.71013786	1.95E-05	0.00040271
ITGA2	0.46289456	2.75E-03	0.01610079
HLA-DMA	0.55430088	5.51E-08	3.93E-06
FLT3LG	0.4490659	9.61E-03	0.04139419
HLA-DPA1	0.92938676	1.37E-05	0.00030788
TNFSF13B	0.69860489	1.28E-04	0.00161705
DPP4	-0.9443008	9.09E-03	0.03959375
CD2	0.50826695	1.20E-03	0.00924521
ITGB2	0.55424083	1.84E-06	6.89E-05
CD74	0.46141186	3.37E-04	0.00367032
CD3E	0.80863298	1.71E-06	6.89E-05
DNAJC14	-0.5333717	5.18E-03	0.02622498
ZNF346	0.42545459	3.18E-03	0.01834309
GPATCH3	-0.4016687	9.89E-03	0.04209206

Supplemental material
BMJ Publishing Group Limited (BMJ) disclaims all liability and responsibility arising from any reliance
placed on this supplemental material which has been supplied by the author(s)
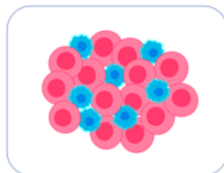Immunother Cancer

The tumor immune microenvironment of primary prostate cancer with and without germline mutations in homologous recombination repair genes

Germline mutations
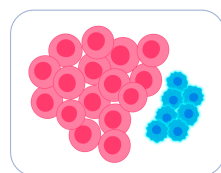*BRCA2, BRCA1,*
ATM, FANCI, PALB2,
CHEK2, MSH2

Sporadic

Similar density and composition of T cells
Distinct immune spatial profiles

Free immune spatial (FIS) profile

Clustered immune spatial (CIS) profile

CD8$^+$ cells in close
proximity to tumor cells
Higher HLA-A

Clusters of CD4$^+$ T cells
closely interacting with
PD-L1$^+$ cells

Authors

Anna S. Trigos, Anupama Pasam, Patricia Banks, Roslyn Wallace, Christina Guo, Simon P. Keam, Heather Thorne, kConFab, Catherine Mitchell, Stephen Lade, David Clouston, Alexander Hakansson, Yang Liu, Benjamin Blyth, Declan G. Murphy, Nathan Lawrentschuk, Damien Bolton, Daniel Moon, Phil K. Darcy, Ygal Haupt, Scott Williams, Elena Castro, David Olmos, David L. Goode, Paul J. Neeson, Shahneen Sandhu

Correspondence

Shahneen.Sandhu@petermac.org

In Brief

The T cell immune microenvironment of primary prostate cancer tumors can show enrichment of CD8$^+$ T cells closely interacting with tumour cells, which we define as a Free Immune Spatial (FIS) profile, or clustering of CD4$^+$ T cells, which we define as a Clustered Immune Spatial (CIS) profile. The former was mainly found in tumours from patients with germline mutations in homologous recombination repair genes. A FIS profile is linked to longer time to biochemical recurrence, metastasis, smaller tumor size and lower Gleason scores.